THE ASTROPHYSICAL JOURNAL SUPPLEMENT SERIES, 77:255–285, 1991 October

MOLECULAR LINE SURVEY OF SAGITTARIUS B2(M) FROM 330 TO 355 GHz AND COMPARISON WITH SAGITTARIUS B2(N)

E. C. SUTTON,[1,2] P. A. JAMINET,[2] AND W. C. DANCHI
Department of Physics and Space Sciences Laboratory, University of California, Berkeley, CA 94720

AND

GEOFFREY A. BLAKE
Division of Geological and Planetary Sciences, MC 107-25, California Institute of Technology, Pasadena, CA 91125
Received 1990 December 4; accepted 1991 March 26

ABSTRACT

We have surveyed molecular line emission from Sgr B2 over the range from 330 to 355 GHz at the position designated Sgr B2(M). This position is prominent in millimeter continuum maps of the region and is associated with a compact H II region, a hot NH_3 core, and sources of H_2O and OH maser emission. We have also obtained observations contrasting the submillimeter molecular emission from Sgr B2(M) and Sgr B2(N), an additional center of activity thought to be a dense protostellar core.

The picture of the interstellar chemistry of these regions which we derive is substantially different from that determined from previous observations at lower frequencies and with lower spatial resolution. In particular, molecules such as SO_2 and CH_3OH dominate the submillimeter spectrum to a much greater extent than they do the low-frequency observations. Much of this difference is due to the higher spatial resolution of the submillimeter observations, which makes them much more sensitive to emission from compact, dense cores. The millimeter data were most effective at sampling material in the surrounding lower density regions. The chemistry of the core sources in Sgr B2 appears similar to that of other dense cores, such as the core of the Orion molecular cloud.

The spectral differences between Sgr B2(M) and Sgr B2(N) primarily relate to differences in excitation and column density. For most molecular species the northern source (N) has a column density significantly higher than that found in the middle source (M), often by a factor of about 5. The principal exceptions are the species SO and SO_2 which seem to be substantially more abundant in the middle source. Generally excitation seems to be higher in the northern source, suggesting a somewhat higher density core, although there are some departures indicating that the excitation situation is more complicated. High optical depths in many of the submillimeter transitions systematically bias the interpretation of both column densities and excitation. Many of the millimeter lines may also have high optical depths, particularly those lines arising from the compact core sources.

Subject headings: interstellar: abundances — interstellar: molecules — line identifications — masers —nebulae: individual (Sgr B2)

1. INTRODUCTION

For the study of interstellar molecules, the giant molecular cloud Sgr B2 is the largest, richest, and most chemically diverse region known in the Galaxy. Many interstellar molecules were first detected in Sgr B2, and a number have still been seen only in this source. The earliest spectral survey work on Sgr B2 was the 3 mm Bell Telephone Laboratories (BTL) survey of Cummins, Linke, & Thaddeus (1986), which detected 457 lines arising from at least 39 different species. More recent 3 mm survey work at the National Radio Astronomy Observatory (NRAO) by Turner (1989, 1991) has resulted in the detection of over 700 lines. Surveys of this sort are particularly valuable in that detection of multiple lines of a given chemical species helps one determine excitation conditions and thereby obtain more accurate molecular abundances.

Observations of Sgr B2 with high spatial resolution have revealed that there is considerable small-scale structure. Goldsmith et al. (1987) have used the Nobeyama 45 m telescope to map a number of molecular transitions, and have shown that lines of various molecular species exhibit remarkably different spatial distributions. In particular, some lines peak strongly on the northern (N) H_2O maser position, whereas others peak around the middle (M) H_2O maser source. To some extent this can be attributed to excitation, as in the case of vibrationally excited HC_3N and possibly HNCO. However, Goldsmith et al. conclude that there must be variations in molecular abundances as well. For our understanding of interstellar chemistry it is important to confirm to what extent such variations are related to true abundance variations as opposed to differences in excitation.

Interferometric studies have added considerable additional detail about small-scale structure. VLA measurements by Vogel, Genzel, & Palmer (1987) have shown the existence of two hot NH_3 cores, associated with the northern and middle H_2O maser positions. The northern core was found to be particularly massive, both in NH_3 and in the millimeter continuum emission mapped by Carlstrom & Vogel (1989), who have

[1] Also Departments of Astronomy and Electrical and Computer Engineering, University of Illinois at Urbana-Champaign.
[2] Postal address: Department of Astronomy, University of Illinois, 1002 W. Green Street, Urbana, IL 61801.

argued that the dust emission in the north arises from a dense and massive protostellar core. Ongoing work includes high-resolution maps of a number of millimeter-wave molecular transitions (Snyder, Kuan, & Pratap 1991; Lis et al. 1991).

In this work we describe the first submillimeter spectral survey of Sgr B2 and the first survey with sufficient spatial resolution to resolve some of the known source structure. There are several predictable characteristics of high-frequency surveys. One is that optical depths in the submillimeter range will, in general, be larger than at millimeter wavelengths, assuming there is sufficient excitation to significantly populate the levels. At high frequencies the spectrum will also become increasingly dominated by emission from relatively light rotors with significant *b*-axis dipole components. For heavy rotors with pure *a*-type spectra (e.g., HC_7N) the only lines occurring in the submillimeter will involve levels with very high excitation energies, which are difficult to populate. Finally, the high optical depths and the presence of significant continuum emission will give rise to complex (self-absorbed) line shapes. These will contain considerable information about the line-of-sight structure of the source, but will be difficult to interpret.

2. OBSERVATIONS

Sagittarius B2 is a large region with complex structure, some of which can be easily resolved in single-dish observations. There are three main centers of activity, arranged in a rough north-south line. Each of these centers is associated with a complex of H_2O maser sources (Elmegreen et al. 1980) and with one or more compact H II regions. The northern (N) and middle (M) sources are the most prominent in centimeter and millimeter continuum maps and are thought to be regions of very high luminosity. Both are coincident with hot NH_3 cores. The middle (M) and southern (S) positions are coincident with OH maser activity. The positions we have adopted for these sources are listed in Table 1. We have chosen to concentrate on Sgr B2(M) and Sgr B2(N), which are the regions of highest luminosity and greatest column density and therefore of greatest interest in the study of massive star formation. Previous molecular surveys have been centered on a position between Sgr B2(M) and Sgr B2(S), generally known as Sgr B2(OH). These earlier surveys had sufficiently large beams to encompass both Sgr B2(M) and Sgr B2(S) and, at times, parts of Sgr B2(N).

The observations reported here were conducted in two parts. The first part, a spectral survey from 330 to 355 GHz, was carried out at the Caltech Submillimeter Observatory (CSO) during 1988 June and July. At these frequencies the 10.4 m CSO provided a beam size of about 20″ FWHM. With this resolution it was our original intent to obtain parallel surveys of Sgr B2(M) and Sgr B2(N). In retrospect it appears that our observations of only Sgr B2(N) were mispointed by approximately 10″. Since the northern source is quite compact, this pointing error is sufficiently large for us to mistrust that portion of the observations. The CSO data reported here will therefore be confined to the survey at the middle position. A preliminary discussion of these observations was given by Sutton et al. (1990a).

TABLE 1

ADOPTED SOURCE POSITIONS

Source	α(1950)	δ(1950)
Sgr B2(N)	$17^h44^m10^s.0$	−28°21′15″
Sgr B2(M)	17 44 10.5	−28 22 05
Sgr B2(OH)	17 44 11.0	−28 22 30
Sgr B2(S)	17 44 10.5	−28 22 44

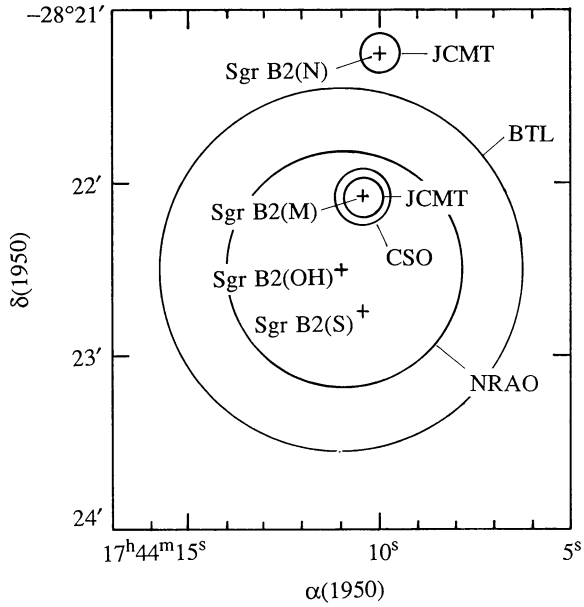

FIG. 1.—Relative positions of Sgr B2(S), Sgr B2(M), and Sgr B2(N). The larger circles illustrate beam sizes of the NRAO (Turner 1989) and BTL (Cummins et al. 1986) surveys, based on median frequencies of 92 and 102 GHz, respectively. Both of these surveys were centered on the position known as Sgr B2(OH). Smaller circles exhibit the beams obtained in this work with the CSO and the JCMT.

To complement this survey of Sgr B2(M), we subsequently used the James Clerk Maxwell Telescope (JCMT) to compare the emission from Sgr B2(M) and Sgr B2(N) in selected passbands. The JCMT observations were obtained during 1989 August. The limited spectral coverage of these observations in part overlapped the region covered in the CSO survey, but also included some data in the 320 GHz region. Typical beam size on the 15 m JCMT at these frequencies was 14″ FWHM. In Figure 1 we show a map of Sgr B2 illustrating locations of the various surveys, the sizes of our beams, and the beam sizes of previous surveys.

Both sets of data were obtained using a double-sideband SIS waveguide mixer receiver which has been described in detail by Sutton et al. (1990b). The back-end systems consisted of facility-supplied acousto-optical spectrometers, with resolutions of better than 1 MHz and bandwidths of approximately 500 MHz. In both cases the observations were obtained in a position-switched mode with cycle times of 20 s on source and 20 s off source. Total on-source integration time was typically 240 s. Reference positions were symmetrically offset by ±30′ in azimuth. Calibration was obtained using the chopper-wheel method in which the observations are compared with the signal from an ambient temperature load. Telescope efficiencies were obtained by measurements of the Moon and planets. All

data reported here have been reduced to the T_R^* scale by dividing by an extended source (Moon) efficiency of 0.68 (CSO) or 0.72 (JCMT). For the epoch of these observations, main-beam brightness temperatures can be obtained by multiplying these results by a factor of 1.9 (CSO) or 1.3 (JCMT).

The CSO survey was obtained using 82 discrete local oscillator settings, separated typically by 250 MHz. This provided an overlapping and highly redundant data set. These double-sideband observations were then transformed into single-sideband spectra following the general procedure described by Sutton et al. (1985). In this procedure a feature in one of the double-sideband spectra was attributed to either the upper or the lower sideband based on the appearance of other spectra with overlapping frequency coverage. The reliability of the deconvolution is greatest where the redundancy of the data set is largest. Over much of the CSO passband the spectral redundancy (number of observations with different local oscillator settings) averages 3–4, and features in the single-sideband spectrum are generally reliable down to about 0.3 K. Near the edges of the passband, below 333 GHz and above 348 GHz, the redundancy is typically 2 and the single-sideband spectrum is generally reliable at the 0.5 K level.

3. ANALYSIS OF SURVEY DATA FROM SAGITTARIUS B2(M)

The spectrum obtained from the CSO survey of Sgr B2(M) is plotted in Figure 2 in deconvolved single-sideband form. Table 2 is a listing of 128 strong, resolved features in the spectrum, most of which are identified. The spectrum is dominated by emission from SO_2 and CH_3OH, both of which are abundant asymmetric tops with rich spectra. A great variety of line shapes are present. These range from almost pure emission lines, to emission lines with strong central self-reversals, to lines seen almost purely in absorption. Integrated intensities have been calculated for those lines seen predominantly in emission.

We use a number of techniques to analyze these observations. For those molecules with sufficient numbers of observed lines, we first examine the data using the rotation diagram technique. If line opacities are low and the molecular excitation is thermal, we can use this technique to determine column densities and excitation temperatures. If these conditions are not true, the rotation diagram still provides limited information on opacities and excitation. In some cases isotopic emission provides important additional information about line opacities. For species with few observable lines at these frequencies, we compare our results with the intensities expected based on abundances and excitation temperatures derived from previous lower frequency surveys. Finally, in a few cases we use line-shape information to determine source structure and variations in the properties of the molecular material.

The rotation diagram technique is based on the assumption that the populations of the various molecular levels correspond to local thermodynamic equilibrium (LTE) at some rotational temperature $T_{\rm rot}$. For transitions which are optically thin the equations of radiative transfer can be integrated to obtain a relationship between the logarithm of the integrated line intensity and the energy of the upper state. From measurements of a number of lines it is then possible to derive the total molecular column density and the rotational temperature. This relationship may be written as

$$\ln\left(\frac{3kc\int T_R^* d\nu}{8\pi^3\nu^2\mu^2 S g_K g_I}\right) = \ln\left[\frac{N_T}{Q(T_{\rm rot})}\right] - \frac{E_u}{kT_{\rm rot}}, \qquad (1)$$

where $\int T_R^* d\nu$ is the integrated intensity, N_T is the molecular column density, Q is the rotational partition function, E_u is the upper state energy, and μ is the appropriate inertial axis component of the permanent dipole moment. Following Turner (1991), we have chosen to display explicitly the K-level degeneracy, g_K, and the nuclear spin degeneracy, g_I, thereby leaving the line-strength parameter S in its normal (e.g., asymmetric rotor) form. It is important that the treatment of degeneracies be the same on both sides of this equation, that is, that the values of $g_K g_I S$ be consistent with the value of the partition function Q. The rotation diagram technique consists of the use of equation (1) to generate a semilogarithmic plot of integrated intensity versus energy. If the initial assumptions of LTE and low optical depth are correct, the data are expected to fall on a straight line. The slope of the line then corresponds to the rotational temperature, and the intercept can be used to derive the molecular column density.

In the discussion which follows, we begin by examining the two molecules whose emission dominates the spectrum of Sgr B2(M), SO_2, and CH_3OH. These molecules have a sufficient number of observed transitions to construct full rotation diagrams. Following these, we will treat, in order of increasing molecular complexity, the remaining molecules which have been detected.

3.1. SO_2 *and* $^{34}SO_2$

We apply the rotation diagram method first to the dominant isotopic species of sulfur dioxide, $^{32}SO_2$, which is seen in a total of 21 transitions in the ground vibrational state, 17 of them unblended. Intensities of three additional transitions have been recovered from partial blends. These data are tabulated in Table 3 and plotted in Figure 3*a*. There is considerable scatter, indicating the likely breakdown of either the assumption of LTE or that of low optical depth. Temporarily ignoring such deviations, one can derive a formal rotational temperature of 166 ± 9 K and a beam-averaged column density of 1.19 ± 0.11 10^{16} cm^{-2} ($1\ \sigma$ error limits).

Turner (1991), in analyzing the NRAO survey data of Sgr B2 and Orion–KL, has described a number of species (not, however, including SO_2) in which the weaker transitions are found to lie systematically high in rotation diagram plots. We see a similar effect in our SO_2 data, with those points with small values of the quantity $S\mu^2$ falling systematically higher in the rotation diagram than those with large values of $S\mu^2$. Turner suggests that behavior of this sort may be explained either by "pumping" of these small $S\mu^2$ transitions, via a radiative bottleneck mechanism, or by large optical depths. The latter explanation is favored in the present case, as will be seen by considering the $^{34}SO_2$ data. If this is correct, the more optically thin lines (those with smaller values of $S\mu^2$) provide a better measure of column density and excitation than the data set as a whole. A rotation diagram fit to just the $^{32}SO_2$ data with $S < 2.5$ yields a rotational temperature of 153 ± 21 K and a column density of 2.48 ± 0.45 10^{16} cm^{-2}.

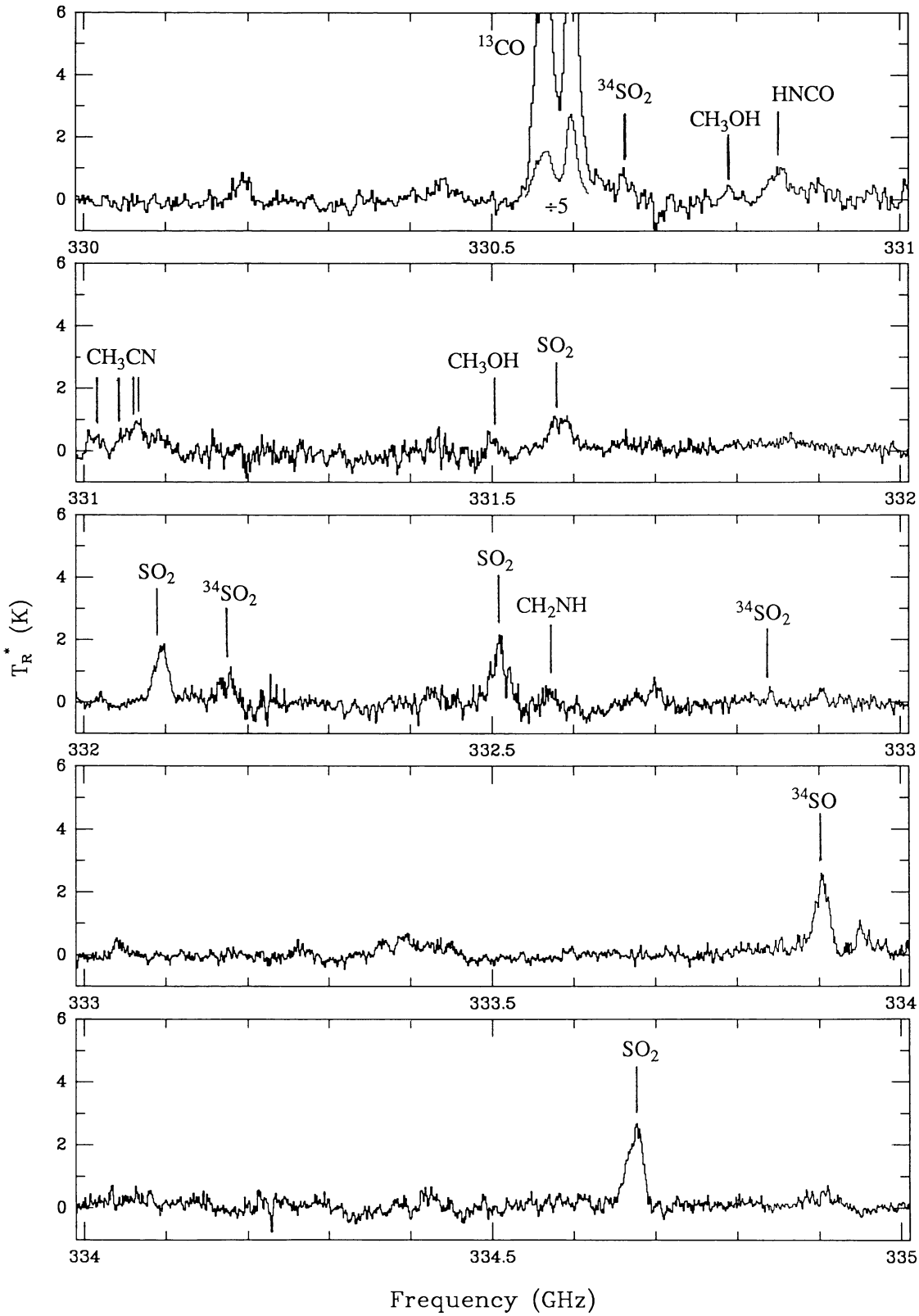

FIG. 2.—Single-sideband spectrum of Sgr B2(M) from 330 to 355 GHz. The scale of rest frequency presumes a v_{lsr} of 61 km s^{-1}. Antenna temperature is given by $T_R^* = T_A^*/\eta_{fss}$ (fss = forward spillover and scattering).

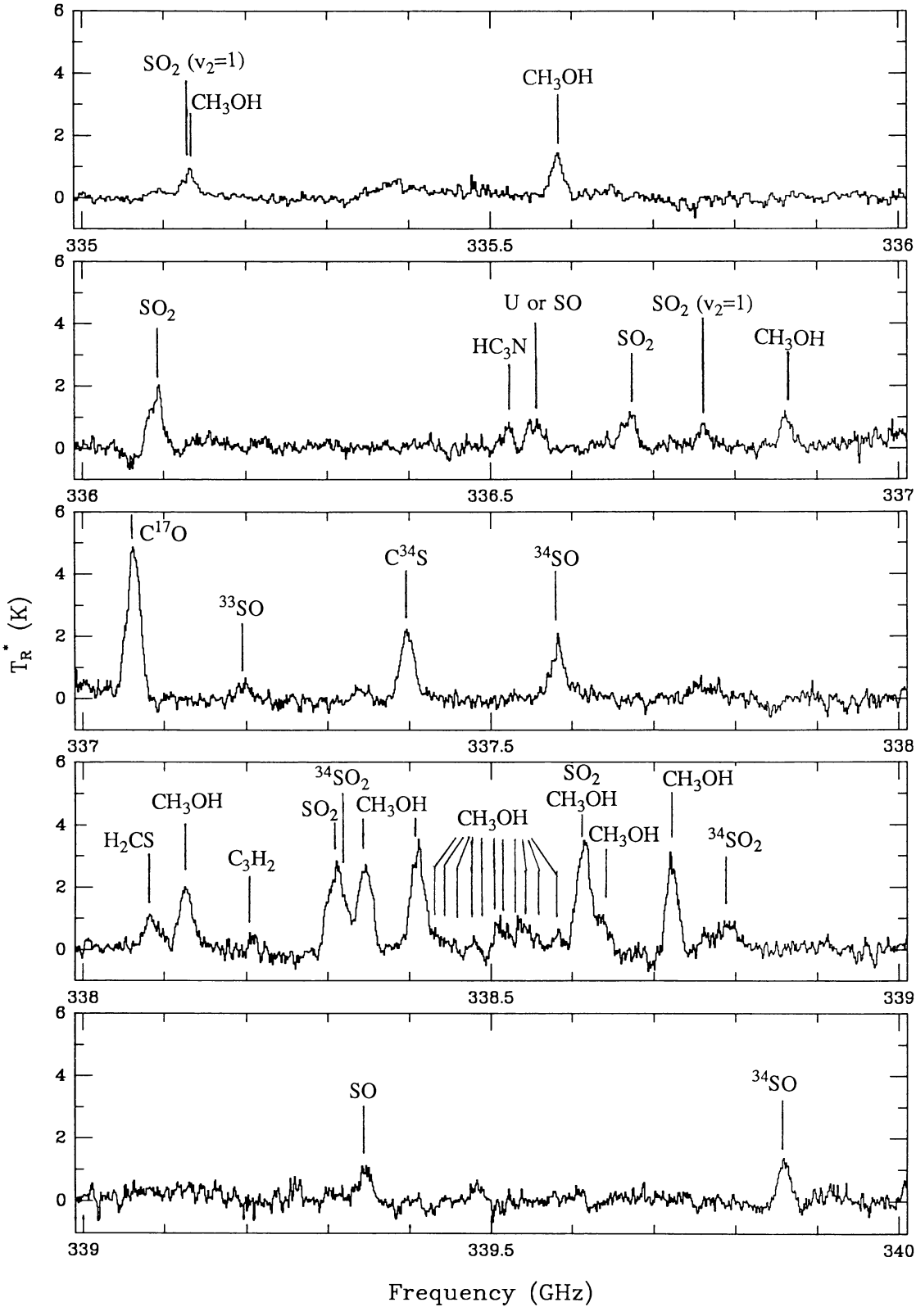

FIG. 2—*Continued*

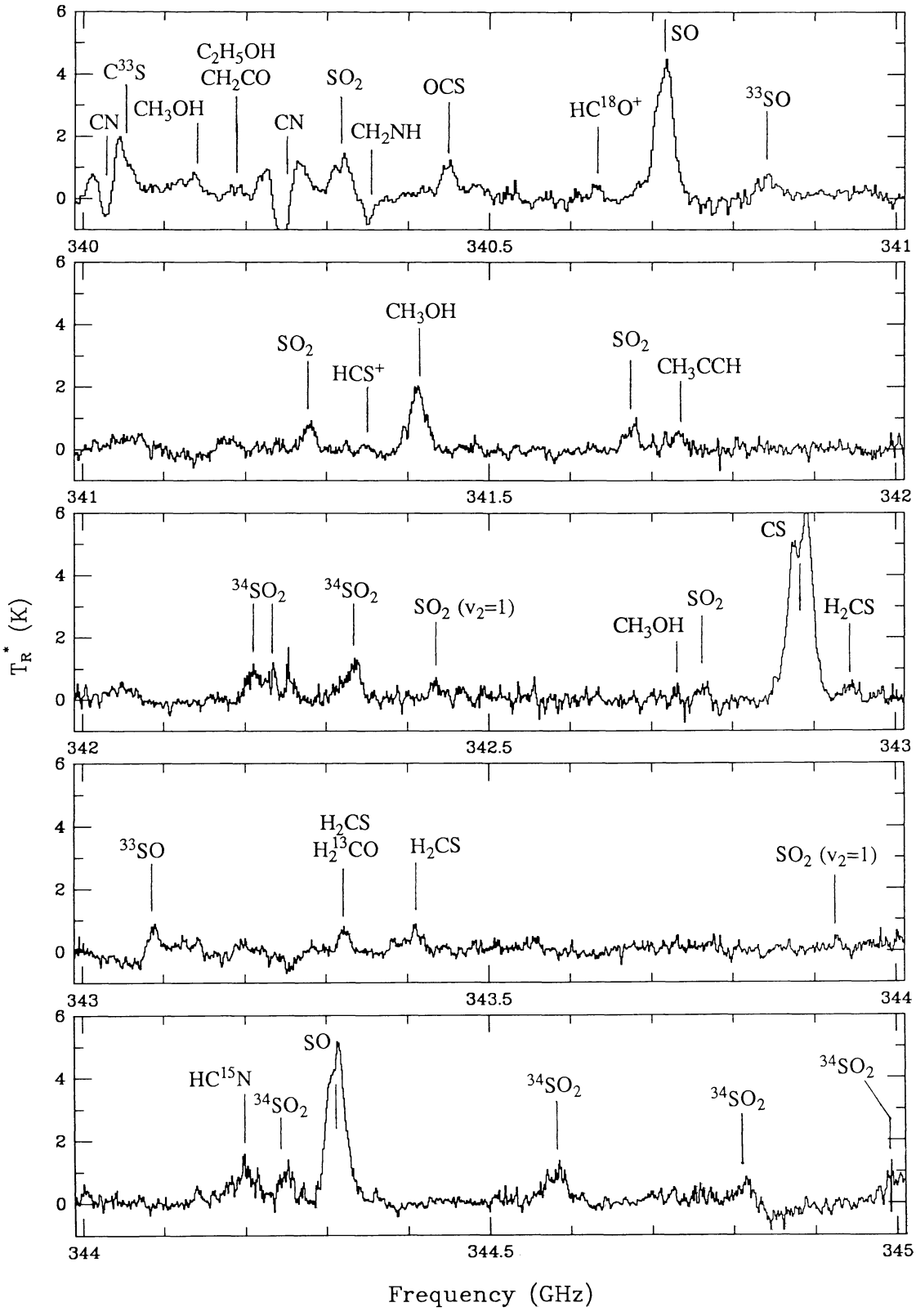

FIG. 2—*Continued*

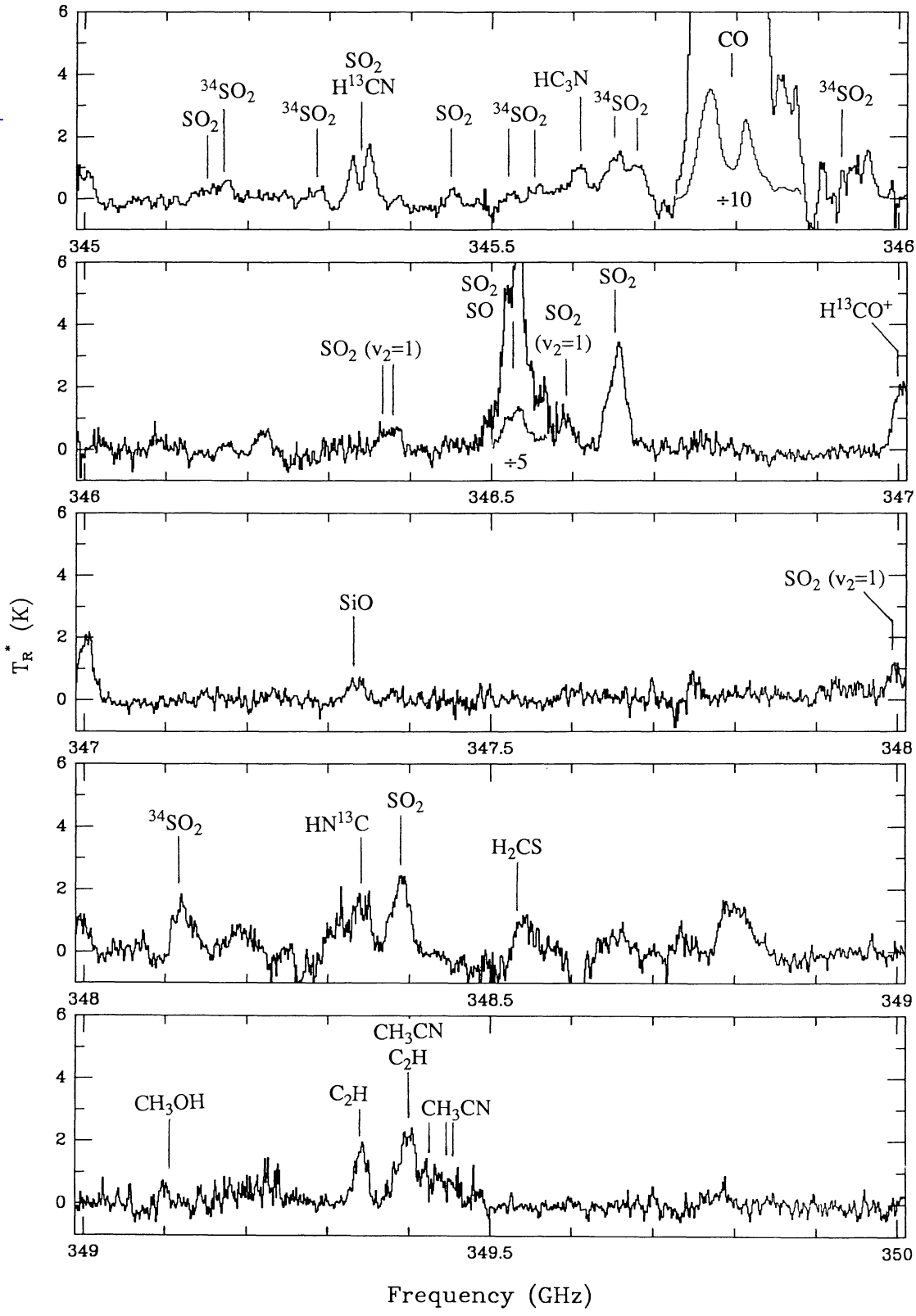

FIG. 2—*Continued*

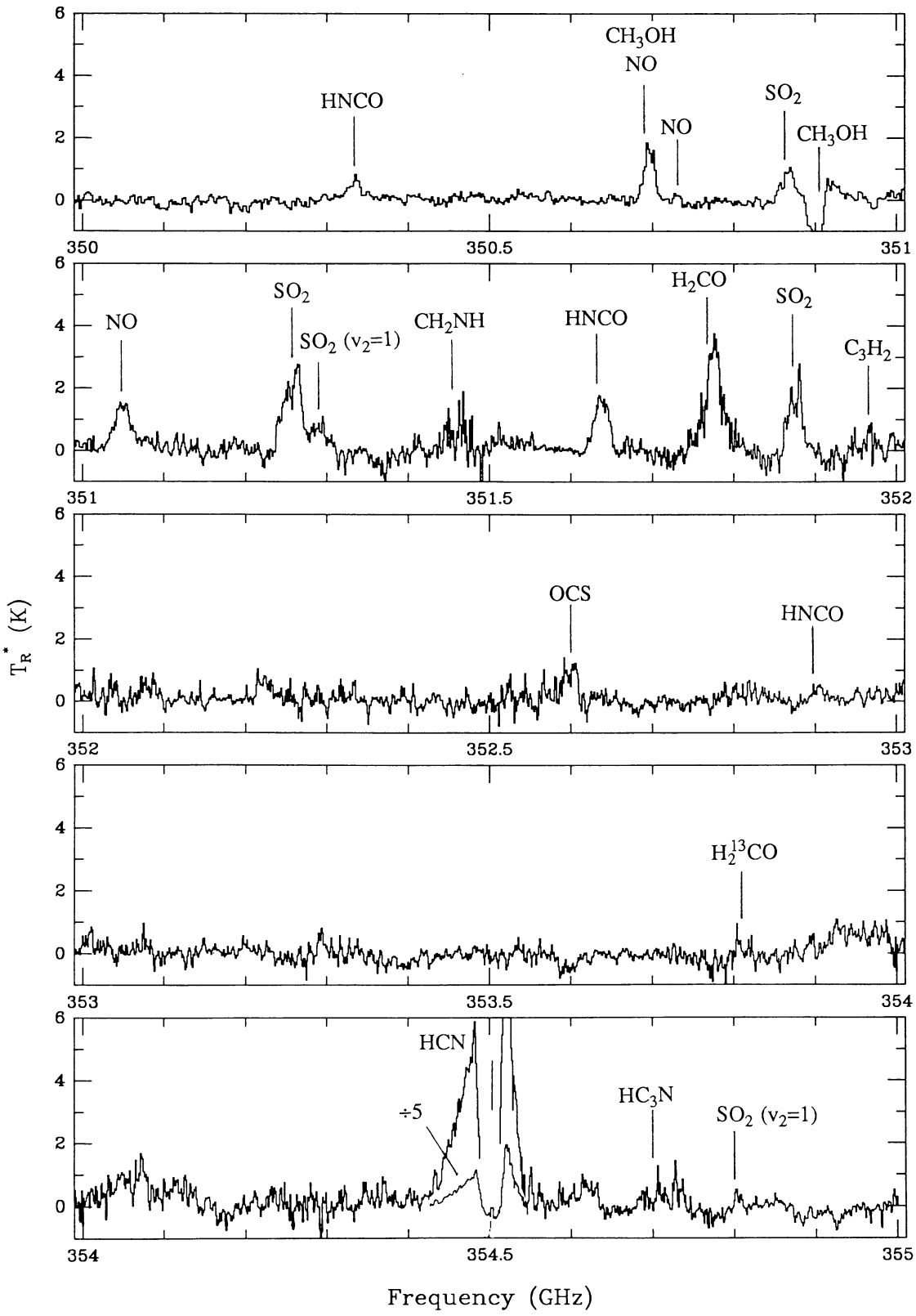

FIG. 2—*Continued*

TABLE 2

LINES DETECTED IN SAGITTARIUS B2(M)

Frequency (MHz)	Species	Transition
330588.0	^{13}CO	3-2
330667.6	$^{34}SO_2$	$21_{2,20}$–$21_{1,21}$
330793.9	CH_3OH	8_{-3}–9_{-2} E
330848.8	HNCO	$15_{1,14}$–$14_{1,13}$
331014.1	CH_3CN	18_3–17_3
331045.9	CH_3CN	18_2–17_2
331065.0	CH_3CN	18_1–17_1
331071.3	CH_3CN	18_0–17_0
331502.4	CH_3OH	11_1 A$^-$–11_0 A$^+$
331580.2	SO_2	$11_{6,6}$–$12_{5,7}$
332091.4	SO_2	$21_{2,20}$–$21_{1,21}$
332173.7	$^{34}SO_2$	$23_{3,21}$–$23_{2,22}$
332505.2	SO_2	$4_{3,1}$–$3_{2,2}$
332572.8	CH_2NH	$5_{1,4}$–$4_{1,3}$
332836.3	$^{34}SO_2$	$16_{4,12}$–$16_{3,13}$
333901.0	^{34}SO	8_7–7_6
334673.3	SO_2	$8_{2,6}$–$7_{1,7}$
335128.5	SO_2 (v_2=1)	$20_{4,16}$–$20_{3,17}$
335133.5	CH_3OH	2_2–3_1 A$^-$
335582.0	CH_3OH	7_1–6_1 A$^+$
336089.2	SO_2	$23_{3,21}$–$23_{2,22}$
336521.0	HC_3N	37-36
336553.	U or SO	
336669.6	SO_2	$16_{7,9}$–$17_{6,12}$
336760.7	SO_2 (v_2=1)	$20_{1,19}$–$19_{2,18}$
336865.1	CH_3OH	12_1 A$^-$–12_0 A$^+$
337061.1	$C^{17}O$	3-2
337195.	^{33}SO	8_7–7_6
337396.6	$C^{34}S$	7-6
337579.3	^{34}SO	8_8–7_7
338080.8	H_2CS	$10_{1,10}$–$9_{1,9}$
338124.5	CH_3OH	7_0–6_0 E
338204.0	C_3H_2	$5_{5,1}$–$4_{4,0}$
338306.0	SO_2	$18_{4,14}$–$18_{3,15}$
338320.4	$^{34}SO_2$	$13_{2,12}$–$12_{1,11}$
338344.6	CH_3OH	7_{-1}–6_{-1} E
338404.6	CH_3OH	7_6–6_6 E
338408.7	CH_3OH	7_0–6_0 A$^+$
338430.9	CH_3OH	7_{-6}–6_{-6} E
338442.3	CH_3OH	7_6–6_6 A$^\pm$
338456.5	CH_3OH	7_{-5}–6_{-5} E
338475.3	CH_3OH	7_5–6_5 E
338486.3	CH_3OH	7_5–6_5 A$^\pm$
338504.1	CH_3OH	7_{-4}–6_{-4} E
338512.8	CH_3OH	7_4–6_4 A$^\pm$
338512.8	CH_3OH	7_2–6_2 A$^-$
338530.2	CH_3OH	7_4–6_4 E
338540.8	CH_3OH	7_3–6_3 A$^+$
338543.2	CH_3OH	7_3–6_3 A$^-$
338559.9	CH_3OH	7_{-3}–6_{-3} E
338583.2	CH_3OH	7_3–6_3 E
338611.8	SO_2	$20_{1,19}$–$19_{2,18}$
338615.0	CH_3OH	7_1–6_1 E
338639.9	CH_3OH	7_2–6_2 A$^+$
338721.6	CH_3OH	7_2–6_2 E
338722.9	CH_3OH	7_{-2}–6_{-2} E
338785.8	$^{34}SO_2$	$14_{4,10}$–$14_{3,11}$
339341.5	SO	3_3–2_3
339855.8	^{34}SO	8_9–7_8
340008.2	CN	$3,\frac{5}{2},\frac{5}{2}$ – $2,\frac{3}{2},\frac{5}{2}$
340019.6	CN	$3,\frac{5}{2},\frac{3}{2}$ – $2,\frac{3}{2},\frac{3}{2}$
340031.5	CN	$3,\frac{5}{2},\frac{7}{2}$ – $2,\frac{3}{2},\frac{5}{2}$
340035.4	CN	$3,\frac{5}{2},\frac{3}{2}$ – $2,\frac{3}{2},\frac{1}{2}$
340035.4	CN	$3,\frac{5}{2},\frac{5}{2}$ – $2,\frac{3}{2},\frac{3}{2}$
340052.7	$C^{33}S$	7-6
340141.2	CH_3OH	2_2–3_1 A$^+$
340188.3	C_2H_5OH	$6_{5,2}$–$5_{4,1}$
340188.4	C_2H_5OH	$6_{5,1}$–$5_{4,2}$
340193.2	CH_2CO	$17_{1,17}$–$16_{1,16}$
340247.8	CN	$3,\frac{7}{2},\frac{7}{2}$ – $2,\frac{5}{2},\frac{5}{2}$
340247.8	CN	$3,\frac{7}{2},\frac{9}{2}$ – $2,\frac{5}{2},\frac{7}{2}$
340248.6	CN	$3,\frac{7}{2},\frac{5}{2}$ – $2,\frac{5}{2},\frac{3}{2}$
340261.8	CN	$3,\frac{7}{2},\frac{5}{2}$ – $2,\frac{5}{2},\frac{5}{2}$
340265.0	CN	$3,\frac{7}{2},\frac{7}{2}$ – $2,\frac{5}{2},\frac{7}{2}$
340316.4	SO_2	$28_{2,26}$–$28_{1,27}$
340353.8	CH_2NH	$3_{1,3}$–$2_{0,2}$
340449.3	OCS	28-27
340633.0	$HC^{18}O^+$	4-3
340714.2	SO	8_7–7_6
340839.	^{33}SO	8_8–7_7
341275.5	SO_2	$21_{8,14}$–$22_{7,15}$
341350.8	HCS^+	8-7
341415.6	CH_3OH	7_1–6_1 A$^-$
341674.0	SO_2	$36_{5,31}$–$36_{4,32}$
341734.6	CH_3CCH	20_1–19_1
341741.1	CH_3CCH	20_0–19_0
342208.9	$^{34}SO_2$	$5_{3,3}$–$4_{2,2}$
342231.7	$^{34}SO_2$	$20_{1,19}$–$19_{2,18}$
342332.1	$^{34}SO_2$	$12_{4,8}$–$12_{3,9}$
342435.9	SO_2 (v_2=1)	$23_{3,21}$–$23_{2,22}$
342729.8	CH_3OH	13_1A$^-$–13_0A$^+$
342761.6	SO_2	$34_{3,31}$–$34_{2,32}$
342882.9	CS	7-6
342944.4	H_2CS	$10_{0,10}$–$9_{0,9}$
343086.	^{33}SO	8_9–7_8
343319.6	H_2CS	$10_{2,9}$–$9_{2,8}$
343325.7	$H_2^{13}CO$	$5_{1,5}$–$4_{1,4}$
343408.1	H_2CS	$10_{3,8}$–$9_{3,7}$
343412.3	H_2CS	$10_{3,7}$–$9_{3,6}$
343923.8	SO_2 (v_2=1)	$24_{2,22}$–$23_{3,21}$
344200.3	$HC^{15}N$	4-3
344245.4	$^{34}SO_2$	$10_{4,6}$–$10_{3,7}$
344310.6	SO	8_8–7_7
344581.1	$^{34}SO_2$	$19_{1,19}$–$18_{0,18}$
344808.0	$^{34}SO_2$	$13_{4,10}$–$13_{3,11}$
344987.7	$^{34}SO_2$	$15_{4,12}$–$15_{3,13}$
344998.3	$^{34}SO_2$	$11_{4,8}$–$11_{3,9}$
345149.0	SO_2	$5_{5,1}$–$6_{4,2}$
345168.8	$^{34}SO_2$	$8_{4,4}$–$8_{3,5}$
345285.7	$^{34}SO_2$	$9_{4,6}$–$9_{3,7}$
345338.5	SO_2	$13_{2,12}$–$12_{1,11}$
345339.5	$H^{13}CN$	4-3
345449.0	SO_2	$26_{9,17}$–$27_{8,20}$
345519.8	$^{34}SO_2$	$7_{4,4}$–$7_{3,5}$
345553.2	$^{34}SO_2$	$6_{4,2}$–$6_{3,3}$
345610.1	HC_3N	38-37
345651.4	$^{34}SO_2$	$5_{4,2}$–$5_{3,3}$
345678.9	$^{34}SO_2$	$4_{4,0}$–$4_{3,1}$
345796.0	CO	3-2
345929.3	$^{34}SO_2$	$17_{4,14}$–$17_{3,15}$
346364.8	SO_2 (v_2=1)	$34_{3,31}$–$34_{2,32}$
346379.3	SO_2 (v_2=1)	$19_{1,19}$–$18_{0,18}$
346523.9	SO_2	$16_{4,12}$–$16_{3,13}$
346528.5	SO	8_9–7_8
346591.8	SO_2 (v_2=1)	$18_{4,14}$–$18_{3,15}$
346652.2	SO_2	$19_{1,19}$–$18_{0,18}$
346998.5	$H^{13}CO^+$	4-3
347330.6	SiO	8-7
347991.8	SO_2 (v_2=1)	$13_{2,12}$–$12_{1,11}$
348117.6	$^{34}SO_2$	$19_{4,16}$–$19_{3,17}$
348340.5	$HN^{13}C$	4-3
348387.8	SO_2	$24_{2,22}$–$23_{3,21}$
348531.9	H_2CS	$10_{1,9}$–$9_{1,8}$
349107.0	CH_3OH	14_1A$^-$–14_0A$^+$
349337.5	C_2H	$4,\frac{9}{2},5$–$3,\frac{7}{2},4$
349338.7	C_2H	$4,\frac{9}{2},4$–$3,\frac{7}{2},3$
349393.0	CH_3CN	19_3–18_3
349398.9	C_2H	$4,\frac{7}{2},4$–$3,\frac{5}{2},3$
349400.3	C_2H	$4,\frac{7}{2},3$–$3,\frac{5}{2},2$
349426.6	CH_3CN	19_2–18_2
349446.7	CH_3CN	19_1–18_1
349453.4	CH_3CN	19_0–18_0
350333.3	HNCO	$16_{1,16}$–$15_{1,15}$
350687.7	CH_3OH	4_0–3_{-1} E
350689.5	NO	$\frac{7}{2},\frac{9}{2}$ – $\frac{5}{2},\frac{7}{2}$ f
350690.8	NO	$\frac{7}{2},\frac{7}{2}$ – $\frac{5}{2},\frac{5}{2}$ f
350694.8	NO	$\frac{7}{2},\frac{5}{2}$ – $\frac{5}{2},\frac{3}{2}$ f
350729.6	NO	$\frac{7}{2},\frac{5}{2}$ – $\frac{5}{2},\frac{5}{2}$ f
350736.8	NO	$\frac{7}{2},\frac{7}{2}$ – $\frac{5}{2},\frac{7}{2}$ f
350862.7	SO_2	$10_{6,4}$–$11_{5,7}$
350905.1	CH_3OH	1_1–0_0 A$^+$
351043.5	NO	$\frac{7}{2},\frac{9}{2}$ – $\frac{5}{2},\frac{7}{2}$ e
351051.7	NO	$\frac{7}{2},\frac{7}{2}$ – $\frac{5}{2},\frac{5}{2}$ e
351051.7	NO	$\frac{7}{2},\frac{5}{2}$ – $\frac{5}{2},\frac{3}{2}$ e
351257.2	SO_2	$5_{3,3}$–$4_{2,2}$
351288.8	SO_2 (v_2=1)	$36_{5,31}$–$36_{4,32}$
351454.3	CH_2NH	$10_{1,9}$–$10_{0,10}$
351633.5	HNCO	$16_{0,16}$–$15_{0,15}$
351768.6	H_2CO	$5_{1,5}$–$4_{1,4}$
351873.9	SO_2	$14_{4,10}$–$14_{3,11}$
351965.8	C_3H_2	$9_{1,8}$–$8_{2,7}$
351965.8	C_3H_2	$9_{2,8}$–$8_{1,7}$
352599.6	OCS	29-28
352897.9	HNCO	$16_{1,15}$–$15_{1,14}$
353811.9	$H_2^{13}CO$	$5_{0,5}$–$4_{0,4}$
354505.5	HCN	4-3
354698.7	HC_3N	39-38
354800.0	SO_2 (v_2=1)	$16_{4,12}$–$16_{3,13}$

TABLE 3

TRANSITIONS OF SO_2 AND $^{34}SO_2$

Species	Frequency (MHz)	Transition	E_L (cm^{-1})	$\int T_R^* dv$ (K km s^{-1})	Notes
SO_2	331580.2	$11_{6,6}$–$12_{5,7}$	92.5	29.1	
	332091.4	$21_{2,20}$–$21_{1,21}$	141.5	27.8	
	332505.2	$4_{3,1}$–$3_{2,2}$	10.7	36.8	
	334673.3	$8_{2,6}$–$7_{1,7}$	18.8	49.0	
	336089.2	$23_{3,21}$–$23_{2,22}$	180.6	32.5	
	336669.6	$16_{7,9}$–$17_{6,12}$	159.1	19.9	
	338306.0	$18_{4,14}$–$18_{3,15}$	125.5	46.7	
	338611.8	$20_{1,19}$–$19_{2,18}$	126.9	52.0	a
	340316.4	$28_{2,26}$–$28_{1,27}$	261.0	31.4	
	341275.5	$21_{8,14}$–$22_{7,15}$	245.2	11.9	
	341674.0	$36_{5,31}$–$36_{4,32}$	460.2	12.5	
	342761.6	$34_{3,31}$–$34_{2,32}$	393.0	6.7	
	345149.0	$5_{5,1}$–$6_{4,2}$	40.7	7.0	b
	345338.5	$13_{2,12}$–$12_{1,11}$	53.1	...	c
	345449.0	$26_{9,17}$–$27_{8,20}$	350.6	7.1	
	346523.9	$16_{4,12}$–$16_{3,13}$	102.8	45.	a
	346652.2	$19_{1,19}$–$18_{0,18}$	105.3	71.2	
	348387.8	$24_{2,22}$–$23_{3,21}$	191.8	53.2	
	350862.7	$10_{6,4}$–$11_{5,7}$	84.8	16.1	
	351257.2	$5_{3,3}$–$4_{2,2}$	13.2	58.5	
	351873.9	$14_{4,10}$–$14_{3,11}$	82.7	40.6	
SO_2 (v_2=1)	335128.5	$20_{4,16}$–$20_{3,17}$	674.	...	c
	336760.7	$20_{1,19}$–$19_{2,18}$	650.	10.2	
	342435.9	$23_{3,21}$–$23_{2,22}$	704.	8.8	
	343923.8	$24_{2,22}$–$23_{3,21}$	715.	3.3	
	346364.8	$34_{3,31}$–$34_{2,32}$	916.	8.6	a
	346379.3	$19_{1,19}$–$18_{0,18}$	628.	8.6	a
	346591.8	$18_{4,14}$–$18_{3,15}$	649.	23.1	
	347991.8	$13_{2,12}$–$12_{1,11}$	576.	19.9	
	351288.8	$36_{5,31}$–$36_{4,32}$	983.	15.0	
	354800.0	$16_{4,12}$–$16_{3,13}$	626.	4.3	
$^{34}SO_2$	330667.6	$21_{2,20}$–$21_{1,21}$	140.9	7.3	
	332173.7	$23_{3,21}$–$23_{2,22}$	179.9	13.6	
	332836.3	$16_{4,12}$–$16_{3,13}$	102.1	2.8	
	338320.4	$13_{2,12}$–$12_{1,11}$	53.0	16.5	
	338785.8	$14_{4,10}$–$14_{3,11}$	82.1	22.2	
	342208.9	$5_{3,3}$–$4_{2,2}$	13.0	17.1	b
	342231.7	$20_{1,19}$–$19_{2,18}$	126.4	10.3	b
	342332.1	$12_{4,8}$–$12_{3,9}$	64.7	25.6	
	344245.4	$10_{4,6}$–$10_{3,7}$	50.0	11.8	
	344581.1	$19_{1,19}$–$18_{0,18}$	104.9	27.1	
	344808.0	$13_{4,10}$–$13_{3,11}$	72.9	12.2	
	344987.7	$15_{4,12}$–$15_{3,13}$	91.4	12.1	a
	344998.3	$11_{4,8}$–$11_{3,9}$	56.9	12.1	a
	345168.8	$8_{4,4}$–$8_{3,5}$	37.8	8.7	b
	345285.7	$9_{4,6}$–$9_{3,7}$	43.5	6.5	
	345519.8	$7_{4,4}$–$7_{3,5}$	32.7	6.0	b
	345553.2	$6_{4,2}$–$6_{3,3}$	28.2	9.0	b
	345651.4	$5_{4,2}$–$5_{3,3}$	24.4	35.0	b,d
	345678.9	$4_{4,0}$–$4_{3,1}$	21.2	15.0	b,d
	345929.3	$17_{4,14}$–$17_{3,15}$	112.5	6.0	d
	348117.6	$19_{4,16}$–$19_{3,17}$	136.2	39.8	

[a] Estimated contribution to blend.
[b] Deconvolved value.
[c] Too heavily blended to estimate intensity.
[d] Line falls within broad wings of CO line.

TABLE 4

TRANSITIONS OF CH_3OH

Species	Frequency (MHz)	Transition	E_L (cm^{-1})	$\int T_R^* dv$ (K km s^{-1})	Notes
CH_3OH	330793.9	8_{-3}–9_{-2} E	90.5	7.8	
	331502.4	11_1 A$^-$–11_0 A$^+$	106.5	12.1	
	335133.5	2_2–3_1 A$^-$	19.9	10.4	
	335582.0	7_1–6_1 A$^+$	43.7	22.8	
	336865.1	12_1A$^-$–12_0A$^+$	125.7	13.5	
	338124.5	7_0–6_0 E	42.8	34.8	
	338344.6	7_{-1}–6_{-1} E	37.6	44.4	
	338404.6	7_6–6_6 E	158.0	2.0	a
	338408.7	7_0–6_0 A$^+$	33.9	58.0	a
	338430.9	7_{-6}–6_{-6} E	165.0	} 5.0	a
	338442.3	7_6–6_6 A$^\pm$	168.5		
	338456.5	7_{-5}–6_{-5} E	119.9	5.0	a
	338475.3	7_5–6_5 E	128.3	} 6.6	
	338486.3	7_5–6_5 A$^\pm$	129.7		
	338504.1	7_{-4}–6_{-4} E	94.8	} 10.4	a
	338512.8	7_4–6_4 A$^\pm$	89.7		
	338512.8	7_2–6_2 A$^-$	60.1	6.9	a
	338530.2	7_4–6_4 E	100.4	4.5	a
	338540.8	7_3–6_3 A$^+$	68.5	} 18.0	a
	338543.2	7_3–6_3 A$^-$	68.5		
	338559.9	7_{-3}–6_{-3} E	77.3	4.0	b
	338583.2	7_3–6_3 E	66.9	14.0	
	338615.0	7_1–6_1 E	48.4	17.0	a
	338639.9	7_2–6_2 A$^+$	60.1	17.3	
	338721.6	7_2–6_2 E	49.2	} 44.8	
	338722.9	7_{-2}–6_{-2} E	51.7		
	340141.2	2_2–3_1 A$^+$	19.7	15.4	
	341415.6	7_1–6_1 A$^-$	44.3	42.7	
	342729.8	13_1A$^-$–13_0A$^+$	146.7	4.1	
	349107.0	14_1A$^-$–14_0A$^+$	169.2	8.5	
	350687.7	4_0–3_{-1} E	13.4	...	c
	350905.1	1_1–0_0 A$^+$	0.	...	d

[a] Estimated contribution to blend.
[b] Deconvolved.
[c] Too blended to deconvolve.
[d] Strongly self-reversed.

We have also detected 21 transitions of $^{34}SO_2$. Of these, 11 are unblended and the intensities of several others are recoverable from blends. Broadly speaking, the position of these isotopic lines on the rotation diagram is only about a factor of 4 below those of the parent species, indicating that the lines of the parent species may be significantly saturated. A typical value for $^{32}S/^{34}S$ in the inner Galaxy is about 18 (Wannier 1980). A comparison of the $^{34}SO_2$ data with just the small $S\mu^2$ data of $^{32}SO_2$ yields an isotopic ratio closer to this value. Taken by itself, the $^{34}SO_2$ rotation diagram yields a rotational temperature of 174 ± 30 K and a $^{34}SO_2$ column density of 2.42 ± 0.35 10^{15} cm^{-2}. There is no evidence for saturation in the $^{34}SO_2$ data. The intensities of the $^{34}SO_2$ lines suggest that $^{33}SO_2$ may also be detectable, although at present frequencies for the $^{33}SO_2$ transitions are not well known.

The column density of 2.48×10^{16} cm^{-2} derived for $^{32}SO_2$ is somewhat larger than the value of 6.0×10^{15} cm^{-2} given by Turner (1991), probably indicating the effects of beam dilution in the larger NRAO beam. Turner's rotational temperature of 232 K is somewhat larger than ours, but probably consistent within the rather large errors. Cummins et al. (1986) fitted a two-component model to their data: a 46 K component with 8.6×10^{14} cm^{-2} and a 210 K component with 4.0×10^{15} cm^{-2}. Again, their lower column densities undoubtedly reflect beam dilution. We see no evidence for a two-component distribution in our data, although the effects of saturation might disguise such trends.

The most heavily saturated SO_2 transition in our data set is $19_{1,19}$–$18_{0,18}$ at 346652.2 MHz. From our derived beam-averaged column density we calculate an optical depth of only 0.11 in this transition for gas dispersed evenly throughout our beam. Our conclusion that there are high optical depths in these transitions implies that much of the SO_2 emission comes

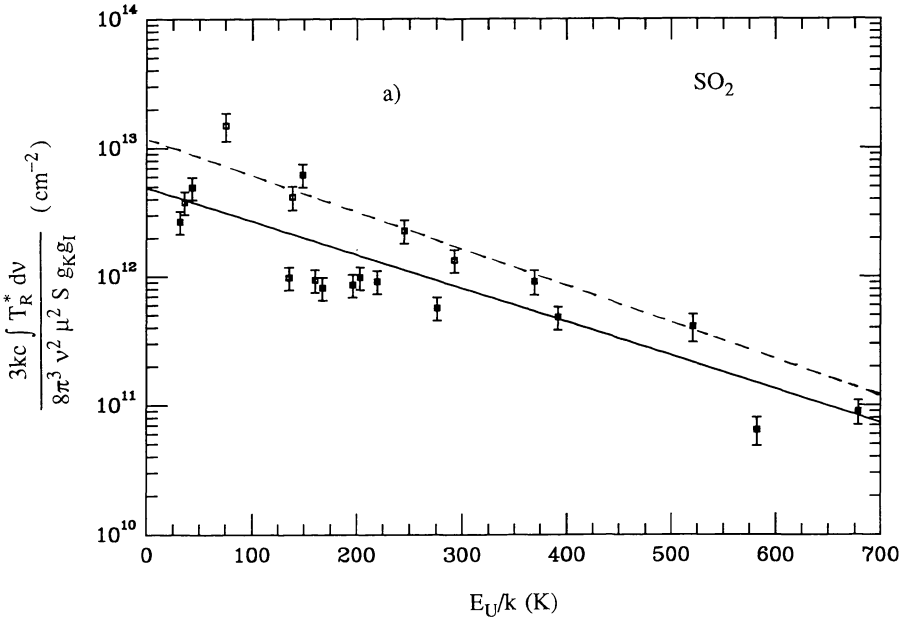

FIG. 3*a*

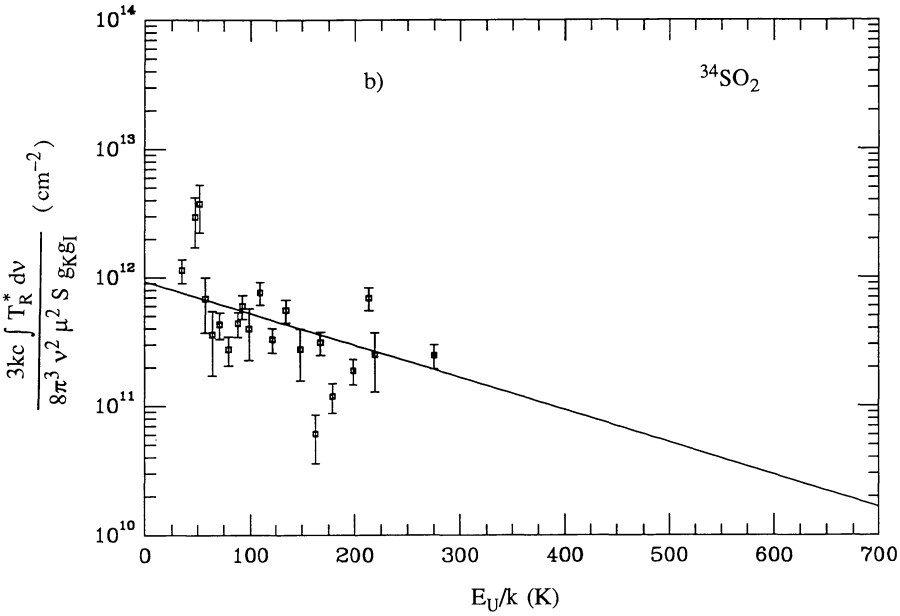

FIG. 3*b*

FIG. 3.—(*a*) Rotation diagram for SO_2. Solid line represents fit to the entire data set; dashed line is a fit to just those data points with line-strength parameter $S < 2.5$. In this and subsequent rotation diagrams, the error bars are a quadrature combination of a 20% systematic uncertainty and a statistical error in the integrated intensity of 1 K km s^{-1} (1 σ). For a variety of reasons (variations in the signal-to-noise ratio, line blending, etc.) this treatment of errors is only approximate, although it should be generally representative of the uncertainties involved. (*b*) Rotation diagram for $^{34}SO_2$. The integrated intensities for the two high-lying $^{34}SO_2$ data points near $E_u/k = 50$ K may be overestimated because of contributions from the wings of the 345796 MHz CO line.

from a compact region unresolved by our 20″ beam (20″ corresponds to 1 pc for a "conventional" distance of 10 kpc). The position of this line in the rotation diagram suggests an optical depth of 4.5, corresponding to a diameter of 3″ for a homogeneous source. This is comparable to the core sizes determined from NH_3 and millimeter continuum data (Vogel et al. 1987; Carlstrom & Vogel 1989).

We also appear to have detected a number of transitions of $^{32}SO_2$ in the $v_2 = 1$ vibrationally excited state. These lines do appear to be somewhat more highly excited than would be expected from a simple extrapolation of the ground-state rotation diagram. As with vibrational bands of other molecules, the population of the vibrationally excited level is likely maintained by radiative excitation in the far-infrared.

3.2. CH_3OH

Emission from methanol in Sgr B2(M) is seen from a number of lines, including those from the strong $J = 7$–6 band near 338.5 GHz. The lines detected range up to an excitation energy of about 250 K, as can be seen from the data in Table 4 and the rotation diagram plot of Figure 4. The intensity falls off fairly rapidly with excitation energy. The best single-component fit to the rotation diagram gives an excitation temperature of 52.8 ± 2.4 K and a column density of $6.85 \pm 0.80\ 10^{15}$ cm^{-2}.

We again see a few systematic deviations in the rotation diagram plot which suggest breakdown of either the assumption of LTE or that of low optical depth. The most prominent deviations are the transitions 2_2–$3_1\ A^{\pm}$. The $2_2\ A^{\pm}$ upper levels are fairly low-lying with excitation energies of about 45 K. These are *b*-type transitions with small line strengths ($\mu^2 S = 0.3$ debye^2). As was the case with SO_2, these transitions lie high on the rotation diagram. The argument of high optical depth, which was used to explain the SO_2 data, is one of three possible explanations for this deviation in CH_3OH. However, high optical depth in CH_3OH seems unlikely, because of our failure to clearly detect both isotopic methanol, $^{13}CH_3OH$, and several other low-line-strength transitions of $^{12}CH_3OH$. A second possibility is a non–LTE distribution of populations. It is known that methanol excitation in general is often non–LTE, as evidenced by the detection of numerous methanol masers. The A species of methanol gives rise to both class A and class B masers (Batrla et al. 1987). The class B masers which have been seen in the torsional ground state of the A species all possess upper levels in the $K = 2$ ladder, indicating a general pattern of overpopulation of $K = 2$ relative to $K = 1$ and $K = 3$. It has been suggested that an excitation pattern of this sort may be created by the $\Delta K = \pm 1$ selection rules for radiative pumping to $v_t = 1$ and subsequent decay to the torsional ground state (Menten et al. 1986a, b). Although there is no direct evidence that this pattern of excitation holds for the $K = 2$ levels in Sgr B2, it is certainly plausible that significantly non–LTE conditions could exist.

A third possibility is that these anomalously strong low-excitation lines could be fitted by invoking a second, cooler component of the gas. Both Turner (1991) and Cummins et al. (1986) employed two-component fits for methanol. Cummins et al. suggested components at 49 and 120 K with column densities of 2.75×10^{16} and 3.5×10^{15} cm^{-2}, respectively. Turner (1991) found a similar strong distinction between cool and hot components, with a break occurring at an excitation energy of around 50 K. His cool component had an excitation temperature of 26 K and a column density of 8.1×10^{15} cm^{-2}. His warm component was fitted by 204^{+392}_{-81} K and 6.9×10^{15} cm^{-2}. Because of our general lack of low-excitation lines, we cannot say much about the cooler component, although our two lowest excitation lines support the existence of such a component. A two-component fit to our data gives temperatures of 17.0 ± 1.6 and 93.1 ± 13.0 K with column densities of $2.49 \pm 0.99 \times 10^{16}$ and $3.57 \pm 0.94 \times 10^{15}$ cm^{-2}, respectively. The column densities are in reasonable agreement with the previous results. Our temperature for the warm component is rather cooler than Turner's 204 K, but the disagreement is not too surprising given his large uncertainties. Our data set contains many more high-energy lines than Turner's and hence better constrains the excitation temperature of the warm component. In this survey we do not detect any emission from the first torsionally excited state, although torsionally excited methanol was seen by Turner (1989).

Goldsmith et al. (1987) detected two methanol lines at the Sgr B2(N) position which they were not able to detect at the Sgr B2(M) position. This is because Sgr B2(N) has both a higher column density of methanol and higher excitation than Sgr B2(M). The lines in question involved levels with excitation energies of about 350 K, and such levels are not well populated in Sgr B2(M). Extrapolating either of our rotation diagram fits, we would predict T_R^* of less than 0.01 K for these

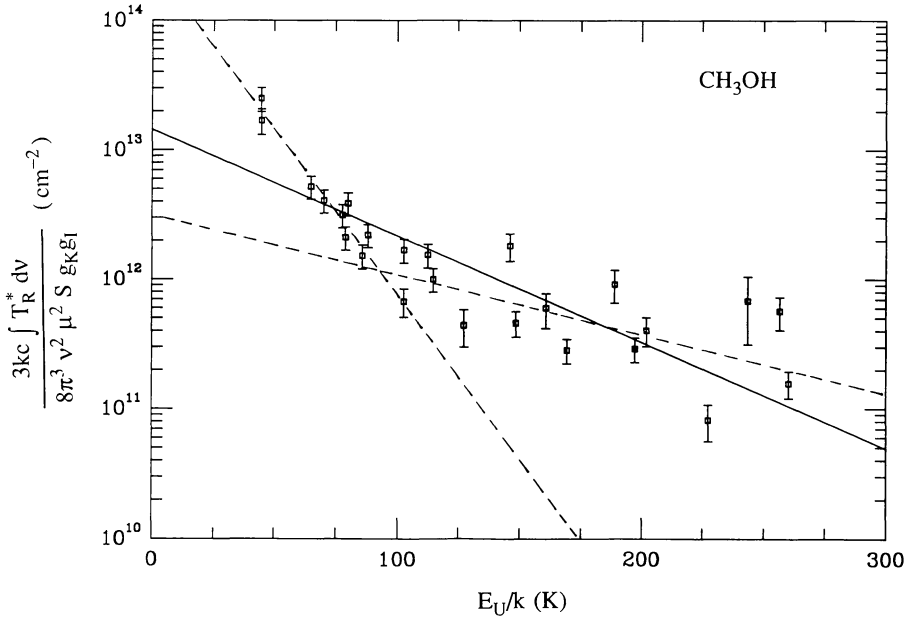

FIG. 4.—Rotation diagram for CH_3OH, showing best single-component fit (*solid line*) and one possible two-component fit (*dashed lines*)

lines in the 15″ Nobeyama beam, which is comparable in size to our CSO beam. It is unlikely that they would have seen lines of this intensity. The differences between Sgr B2(N) and Sgr B2(M) will be discussed more thoroughly in § 4 below.

We have excluded from this analysis one very special line, the 1_1–0_0 A^+ line involving the true ground state of methanol (the 0_0 A^+ level lies 8 K below the 1_{-1} level of the E species). This transition shows a complex line shape with an absorption core extending significantly below the apparent continuum, suggesting significant amounts of cold methanol in the foreground. Other, higher excitation methanol lines typically show little or no self-absorption. Even the 2_2–3_1 $A^{\pm}$ lines show relatively pure emission profiles. The interpretation of the line shape of 1_1–0_0 A^+ will be discussed in § 3.5, in connection with similar absorption features seen in CN.

We have searched for emission from $^{13}CH_3OH$ but failed to find convincing evidence for it. Weak features are present at two of the expected frequencies (330194 and 330442 MHz) but not at a number of other frequencies where equally strong lines also should be present. We are unwilling to attribute these two features to $^{13}CH_3OH$, particularly since they occur near the end of our spectral scan, where the redundancy of the observations is low and the deconvolution of the sidebands less reliable. Our nondetection of $^{13}CH_3OH$ is consistent with the $^{12}CH_3OH$ $J = 7$–6 band being optically thin and an abundance ratio $^{12}CH_3OH/^{13}CH_3OH = 28$.

3.3. CO, CS, SiO, NO, HCN, HNC, HCO^+, *and* HCS^+

In this section we discuss a variety of linear molecules which are observed in only a single J transition. The data for these molecules are tabulated in Table 5. In the absence of excitation information and in order to estimate abundances, we assume (unless otherwise indicated) LTE at 20 K, a temperature representative of a number of species in Sgr B2. Our abundance estimate will be correspondingly uncertain, as is true of any abundance based on a single transition. In cases where, because of high optical depths, we base our abundances on the intensities of isotopic lines, the estimates possess further uncertainties due to possible errors in the assumed isotopic ratios. Finally, for heavy rotors our estimates are based on high-energy transitions and the derived abundance will be strongly dependent on the assumed rotational temperature.

The $J = 3$–2 transition is seen from three isotopic forms of the CO molecule. The ^{12}CO and ^{13}CO lines have complex, self-reversed line shapes, indicative of high optical depths in the foreground gas. In contrast, the $^{12}C^{17}O$ line has a simple pure emission profile. We estimate a column density for $^{12}C^{17}O$ of 4.4×10^{16} cm^{-2}. The $^{16}O/^{17}O$ ratio in the Galactic center has generally been thought to be of order 900 (Wannier 1989). Recent Monte Carlo calculations for Sgr B2 by Lis & Goldsmith (1990) have yielded a $^{13}CO/C^{18}O$ ratio of about 17, a rather lower abundance of ^{18}O than previous estimates. Since the $^{18}O/^{17}O$ ratio is well determined, this suggests that there is less ^{17}O as well. We will adopt a value of $^{16}O/^{17}O \approx 1600$, yielding a CO column density of 7.1×10^{19} cm^{-2}.

The molecule CS is similarly somewhat optically thick in the $J = 7$–6 line of its main isotopic form, $^{12}C^{32}S$. The corresponding line of $C^{34}S$ is easily detected and seems to be optically thin. The species $C^{33}S$ has a line which is blended with the complex CN spectrum just above 340 GHz. Taking only the $C^{34}S$ line and assuming a $^{32}S/^{34}S$ ratio of 18 and a rotational temperature of 20 K, we can estimate a CS column density of 5.9×10^{15} cm^{-2}. If we assume a rotational temperature of 50 K, the derived column density drops to 2.1×10^{15} cm^{-2}.

A single transition of SiO, $J = 8$–7, is seen in these observations. Ziurys, Friberg, & Irvine (1989) have found that SiO is most abundant in high-temperature regions of molecular clouds. However, its excitation may be significantly subthermal. Assuming a rotational temperature of order 50 K, we derive an SiO column density of 2.1×10^{13} cm^{-2}.

For the molecule NO ($^2\Pi_{1/2}$) we have detected several blended hyperfine components of the transition $J = 7/2$–$5/2$. The strongest components of the lower frequency member of the Λ doublet are blended with a CH_3OH line. Rather than attempting to deconvolve those line intensities, we have based our estimate of the NO column density entirely on the emission from the blended hyperfine components near 351050 MHz. We derive a column density of 2.1×10^{16} cm^{-2}.

The $J = 4$–3 lines of HCN and $H^{13}CN$ are strongly self-reversed, indicating high optical depths and a significant amount of HCN in the cool foreground gas. The $HC^{15}N$ line is sufficiently weak to exhibit a simple pure emission-line shape. As with CO and similar species, the estimation of an HCN abundance from a single isotopic line is doubly uncertain, owing to both uncertainties in excitation and uncertainties in isotopic ratios. Assuming our normal excitation temperature of 20 K and an isotopic ratio of $^{14}N/^{15}N = 110$ (Wannier 1989), we derive an HCN column density of 4.4×10^{15} cm^{-2}. For the structural isomer HNC, only the isotopic form $HN^{13}C$ gives a transition in our band. The observed intensity yields a column density of 1.3×10^{15} cm^{-2} assuming $^{12}C/^{13}C = 28$ and excitation as above. Our HNC/HCN abundance ratio of 0.3 is intermediate between values of order unity or greater seen in some cold dark clouds, and much smaller values ($\approx 10^{-2}$ to 10^{-1}) derived for hot molecular cloud cores such as Orion (Goldsmith et al. 1981; Irvine & Schloerb 1984). The smaller ratios are generally attributed to enhanced production of HCN via neutral (atomic) pathways which dominate at high temperatures, an effect which seems to be only moderately present in Sgr B2.

The molecular ion HCO^+ is seen in the forms $H^{13}CO^+$ and $HC^{18}O^+$. The $HC^{18}O^+$ line is sufficiently weak to be unreliable for estimating abundances. We assume $^{12}C/^{13}C = 28$ to estimate an HCO^+ column density of 6.6×10^{14} cm^{-2}. This is based on an HCO^+ dipole moment of 3.91 debye (Botschwina 1989), ignoring isotopic variation in the dipole moment. Normal isotopic HCS^+ is seen in only a single transition. The uncertainty in the derived abundance of 4.7×10^{13} cm^{-2} is dominated by the uncertainty in the excitation temperature, assumed to be 20 K. If the assumed excitation temperature is increased to 50 K, the HCS^+ column density drops to 1.3×10^{13} cm^{-2}.

3.4. SO, ^{34}SO, *and* ^{33}SO

SO is seen in the three J components of $N = 8$–7 and a single low-energy transition (3_3–2_3). There is an additional high-energy transition (11_{10}–10_{10}) at 336553.3 MHz. Emission is seen at this frequency as well, but the observed intensity seems

TABLE 5

ADDITIONAL MOLECULES

Species	Frequency (MHz)	Transition	E_L (cm^{-1})	$\int T_R^* dv$ (K km s^{-1})	Notes
CO	345796.0	3-2	11.5	...	a
^{13}CO	330588.0	3-2	11.0	...	a
$C^{17}O$	337061.1	3-2	11.2	80.5	
CS	342882.9	7-6	34.3	176.4	
$C^{34}S$	337396.6	7-6	33.8	38.7	
$C^{33}S$	340052.7	7-6	34.0	...	b
SiO	347330.6	8-7	40.6	15.4	
SO	336553.3	11_{10}–10_{10}	80.1	16.2	c
	339341.5	3_3–2_3	6.4	17.7	
	340714.2	8_7–7_6	45.1	101.8	
	344310.6	8_8–7_7	49.3	118.5	
	346528.5	8_9–7_8	43.2	152.	d
^{34}SO	333901.0	8_7–7_6	44.4	46.7	
	337579.3	8_8–7_7	48.6	32.5	
	339855.8	8_9–7_8	42.4	22.4	
^{33}SO	337195.	8_7–7_6	45.	9.6	
	340839.	8_8–7_7	49.	16.2	
	343086.	8_9–7_8	43.	11.4	
CN	340008.2	$3,\frac{5}{2},\frac{5}{2}$ – $2,\frac{3}{2},\frac{5}{2}$	11.3	...	a
	340019.6	$3,\frac{5}{2},\frac{3}{2}$ – $2,\frac{3}{2},\frac{3}{2}$	11.3	...	a
	340031.5	$3,\frac{5}{2},\frac{7}{2}$ – $2,\frac{3}{2},\frac{5}{2}$	11.3	...	a
	340035.4	$3,\frac{5}{2},\frac{3}{2}$ – $2,\frac{3}{2},\frac{1}{2}$	11.3	...	a
	340035.4	$3,\frac{5}{2},\frac{5}{2}$ – $2,\frac{3}{2},\frac{3}{2}$	11.3	...	a
	340247.8	$3,\frac{7}{2},\frac{7}{2}$ – $2,\frac{5}{2},\frac{5}{2}$	11.4	...	a
	340247.8	$3,\frac{7}{2},\frac{9}{2}$ – $2,\frac{5}{2},\frac{7}{2}$	11.4	...	a
	340248.6	$3,\frac{7}{2},\frac{5}{2}$ – $2,\frac{5}{2},\frac{3}{2}$	11.4	...	a
	340261.8	$3,\frac{7}{2},\frac{5}{2}$ – $2,\frac{5}{2},\frac{5}{2}$	11.4	...	a
	340265.0	$3,\frac{7}{2},\frac{7}{2}$ – $2,\frac{5}{2},\frac{7}{2}$	11.4	...	a
NO	350689.5	$\frac{7}{2},\frac{9}{2}$ – $\frac{5}{2},\frac{7}{2}$ f	13.4	...	b
	350690.8	$\frac{7}{2},\frac{7}{2}$ – $\frac{5}{2},\frac{5}{2}$ f	13.4	...	b
	350694.8	$\frac{7}{2},\frac{5}{2}$ – $\frac{5}{2},\frac{3}{2}$ f	13.4	...	b
	350729.6	$\frac{7}{2},\frac{5}{2}$ – $\frac{5}{2},\frac{5}{2}$ f	13.4	} 2.3	
	350736.8	$\frac{7}{2},\frac{7}{2}$ – $\frac{5}{2},\frac{7}{2}$ f	13.4		
	351043.5	$\frac{7}{2},\frac{9}{2}$ – $\frac{5}{2},\frac{7}{2}$ e	13.4		
	351051.7	$\frac{7}{2},\frac{7}{2}$ – $\frac{5}{2},\frac{5}{2}$ e	13.4	} 31.7	
	351051.7	$\frac{7}{2},\frac{5}{2}$ – $\frac{5}{2},\frac{3}{2}$ e	13.4		
OCS	340449.3	28-27	153.3	13.3	
	352599.6	29-28	164.7	19.3	
HCN	354505.5	4-3	17.7	...	a
$HC^{15}N$	344200.3	4-3	17.2	37.2	
$H^{13}CN$	345339.5	4-3	17.3	...	a
$HN^{13}C$	348340.5	4-3	17.4	33.9	
HC_3N	336521.0	37-36	202.1	8.3	
	345610.1	38-37	213.3	10.8	
	354698.7	39-38	224.8	7.4	a
$HC^{18}O^+$	340633.0	4-3	17.0	4.9	
$H^{13}CO^+$	346998.5	4-3	17.4	36.7	
HCS^+	341350.8	8-7	39.9	3.5	
C_2H	349337.5	$4,\frac{9}{2},5$–$3,\frac{7}{2},4$	17.5	} 27.6	
	349338.7	$4,\frac{9}{2},4$–$3,\frac{7}{2},3$	17.5		
	349398.9	$4,\frac{7}{2},4$–$3,\frac{5}{2},3$	17.5	...	b
	349400.3	$4,\frac{7}{2},3$–$3,\frac{5}{2},2$	17.5	...	b
CH_3CN	331014.1	18_3–17_3	138.6	11.8	
	331045.9	18_2–17_2	113.8	8.5	
	331065.0	18_1–17_1	98.9	9.5	d
	331071.3	18_0–17_0	93.9	10.2	d
	349393.0	19_3–18_3	149.7	...	b
	349426.6	19_2–18_2	124.8	11.8	
	349446.7	19_1–18_1	109.9	8.9	d
	349453.4	19_0–18_0	104.9	9.5	d
CH_3CCH	341734.6	20_1–19_1	113.3	...	e
	341741.1	20_0–19_0	108.3	...	e
HNCO	330848.8	$15_{1,14}$–$14_{1,13}$	107.3	17.2	
	350333.3	$16_{1,16}$–$15_{1,15}$	117.7	13.1	
	351633.5	$16_{0,16}$–$15_{0,15}$	88.0	29.2	
	352897.9	$16_{1,15}$–$15_{1,14}$	118.4	7.5	
H_2CO	351768.6	$5_{1,5}$–$4_{1,4}$	31.7	66.7	
$H_2^{13}CO$	343325.7	$5_{1,5}$–$4_{1,4}$	31.1	6.0	d
	353811.9	$5_{0,5}$–$4_{0,4}$	23.7	8.2	
H_2CS	338080.8	$10_{1,10}$–$9_{1,9}$	59.9	22.4	
	342944.4	$10_{0,10}$–$9_{0,9}$	51.5	8.2	
	343319.6	$10_{2,9}$–$9_{2,8}$	88.2	3.4	d
	343408.1	$10_{3,8}$–$9_{3,7}$	133.8	} 12.6	
	343412.3	$10_{3,7}$–$9_{3,6}$	133.8		
	348531.9	$10_{1,9}$–$9_{1,8}$	61.5	24.4	
CH_2CO	340193.2	$17_{1,17}$–$16_{1,16}$	99.9	7.1	f
C_3H_2	338204.0	$5_{5,1}$–$4_{4,0}$	22.6	5.3	
	351965.8	$9_{1,8}$–$8_{2,7}$	53.1	} 4.0	
	351965.8	$9_{2,8}$–$8_{1,7}$	53.1		
CH_2NH	332572.8	$5_{1,4}$–$4_{1,3}$	27.7	13.5	
	340353.8	$3_{1,3}$–$2_{0,2}$	6.4	...	g
	351454.3	$10_{1,9}$–$10_{0,10}$	115.4	7.6	
C_2H_5OH	340188.3	$6_{5,2}$–$5_{4,1}$	22.7	} 7.1	h
	340188.4	$6_{5,1}$–$5_{4,2}$	22.7		

[a] Complex shape.
[b] Too heavily blended to estimate intensity.
[c] Uncertain identification.
[d] Estimated contribution to blend.
[e] Very weak.
[f] Blended with C_2H_5OH, fractional contribution unknown.
[g] Seen in absorption.
[h] Blended with CH_2CO, fractional contribution unknown.

anomalously strong. This line will be discussed further below. A rotation diagram incorporating just the other four transitions is shown in Figure 5. This gives a formal fit with a rotation temperature of 23.1 ± 2.5 K and a column density of $6.2 \pm 2.1 \times 10^{15}$ cm^{-2}. In contrast, Cummins et al. report 18.9 K and 4.4×10^{14} cm^{-2}, and Turner gives 14.7 K and 7.7×10^{14} cm^{-2} for temperature and column density, respectively. Our higher column density presumably reflects beam dilution in the NRAO and BTL observations. Our higher temperature may be attributed to the fact that we probe transitions at much higher energies than were previously obtained. We have also observed ^{34}SO in three components of $N = 8$–7, revealing lines with integrated intensities only about a factor of 3.7 below those of ^{32}SO. If the ^{32}S/^{34}S isotopic ratio is of order 18, this indicates that there is considerable saturation in the intensities of the ^{32}SO transitions. Frequencies for the ^{33}SO $N = 8$–7 lines are not well known except for 8_8–7_7, which we appear to have detected. By estimating spin splittings we have also tentatively identified the 8_7–7_6 and 8_9–7_8 transitions of ^{33}SO. The three transitions have similar integrated intensities. Two of these were listed as unidentified lines in the Orion survey of Jewell et al. (1989), where their observed intensities would also be consistent with these identifications. As with ^{34}SO, our detection of ^{33}SO at this level is indicative of a high optical depth in the ^{32}SO lines. Together the ^{34}SO and ^{33}SO data suggest optical depths $\tau \approx 7$ for the ^{32}SO $N = 8$–7 lines and $\tau \approx 0.15$ for the 3_3–2_3 transition. For optically thick lines the integrated intensities need to be corrected upward by the factor $\tau/(1 - e^{-\tau})$ in order to derive column densities using equation (1) and the rotation diagram technique. Correcting the ^{32}SO rotation diagram in this manner yields a rotational temperature of 89 ± 37 K and a column density of $1.3 \pm 0.4 \times 10^{16}$ cm^{-2} (errors do not include allowance for the uncertainty in the optical depth). As corrected in this fashion for high optical depth, the rotation diagram is more consistent with detection of the weak 11_{10}–10_{10} transition, although we still consider that identification questionable. We should note that the high optical depths we derive for ^{32}SO do not conflict with Turner's observation that his SO transitions were optically thin, owing to our much higher frequencies and line strengths.

3.5. CN

The free radical CN is a reactive species thought to exist in relatively low-density regions, often on cloud peripheries where it may be created by UV photolysis of HCN. In our frequency region we are able to examine the fine- and hyperfine-structure multiplets of $N = 3$–2. The strongest members of these multiplets fall into two groups near 340030 and 340250 MHz. For the purposes of Sgr B2 the individual members of these groupings may be viewed as being substantially unresolved. Our observations of these multiplets in Sgr B2(M) are shown in Figure 6, where we have also indicated the locations and relative intensities of the hyperfine components. The line shapes consist of broad emission pedestals with narrow central absorption cores. The absorption cores extend significantly below the level of the continuum and suggest that much of the CN exists as cool foreground gas between us and the continuum source. Three pieces of evidence suggest that this absorption is not saturated. First, the absorption cores do not have flat-bottom profiles. Second, the absorption of the 340250 MHz grouping is deeper, consistent with its greater cumulative line strength. And, finally, we fail to detect any of the weaker hyperfine satellites, the strongest of which has an intensity of 1.2% of that of the entire multiplet. We conclude that the 340250 MHz grouping has an opacity of order unity. The characteristics of the foreground gas are quite uncertain, but assuming it can be described by an excitation temperature of 10 K, we derive a CN column density of order 1.2×10^{15} cm^{-2}.

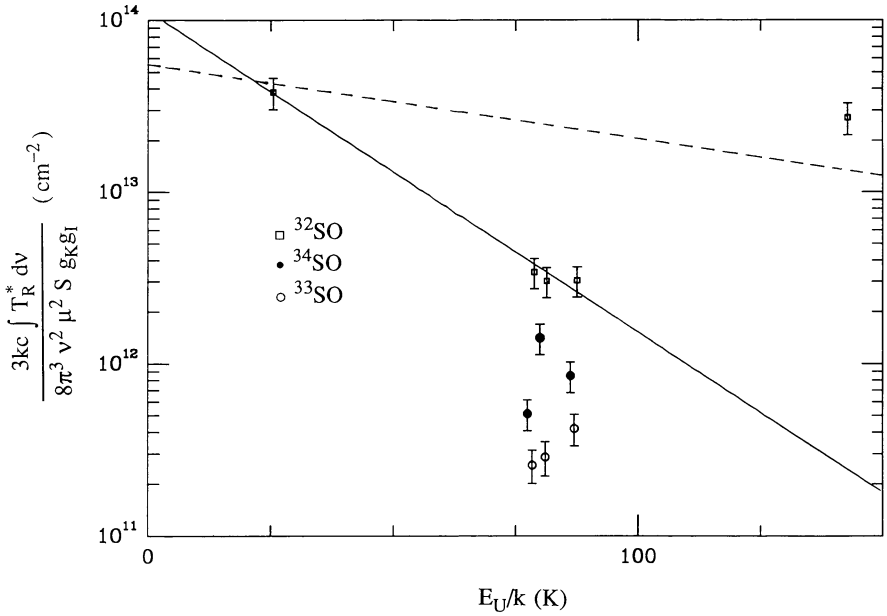

FIG. 5.—Rotation diagram for ^{32}SO (*squares*), ^{34}SO (*filled circles*), and ^{33}SO (*open circles*). Solid line is a fit to the four ^{32}SO transitions (excluding one uncertain identification). Dashed line indicates fit after correction for saturation.

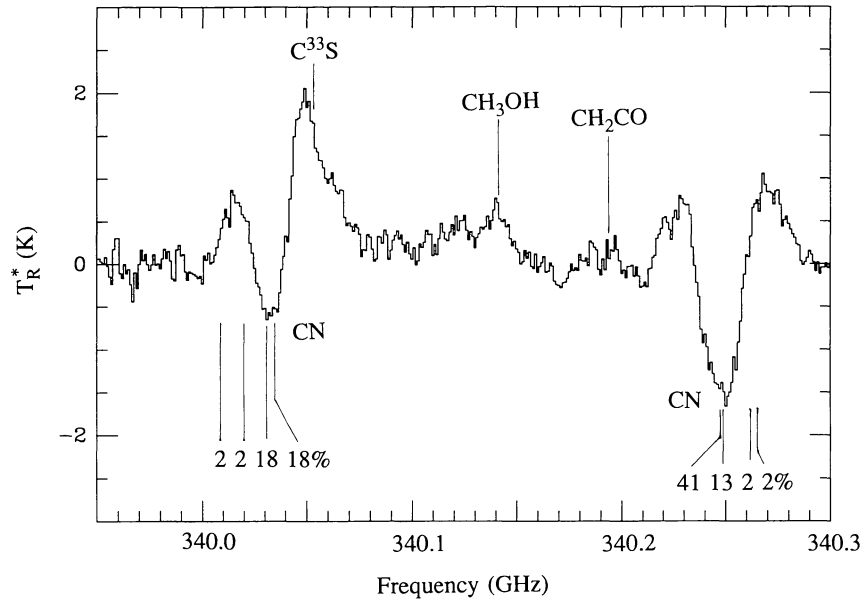

FIG. 6.—Spectrum containing CN $N = 3$–2 multiplet. Markings below the spectrum indicate frequencies of the strongest hyperfine components and relative intensities (as percentages of the strength of the entire transition).

The other feature most similar in appearance to these CN profiles is the 1_1–0_0 A^+ transition of methanol, shown in Figure 7. The absorption extending below the apparent continuum again suggests the presence of very cold gas in the foreground. The profile resembles that of the stronger CN multiplet, suggesting a similar degree of saturation. If we assume an opacity of unity and an excitation temperature of 10 K, we derive a foreground column density of 4×10^{15} cm^{-2}, a significant fraction of all the methanol. While our assumed temperature structure is quite arbitrary, it is clear that the methanol must be distributed in a core/halo type structure with cooler foreground gas overlying the hotter, more active regions of the cloud.

The depths of the CN and CH_3OH absorption features can be compared with previous measurements of the continuum flux. Goldsmith et al. (1990) measured the combined dust and free-free continuum flux density from Sgr B2(M) to be 79 Jy at 1100 μm in a 19″ beam, of which approximately 74 Jy was thought to be due to dust emission. Taking a $\lambda^{-1.3}$ opacity law (cf. Wright & Vogel 1985; Carlstrom & Vogel 1989) and therefore scaling the flux density as $\lambda^{-3.3}$ gives 154 Jy at the CN frequency and 170 Jy at the CH_3OH frequency. Based on our calibration measurements of Mars, an unresolved continuum source, these correspond to a continuum level of $T_R^* \approx 2.6$ K, consistent with our conclusion that the absorption features discussed above have opacities of order unity.

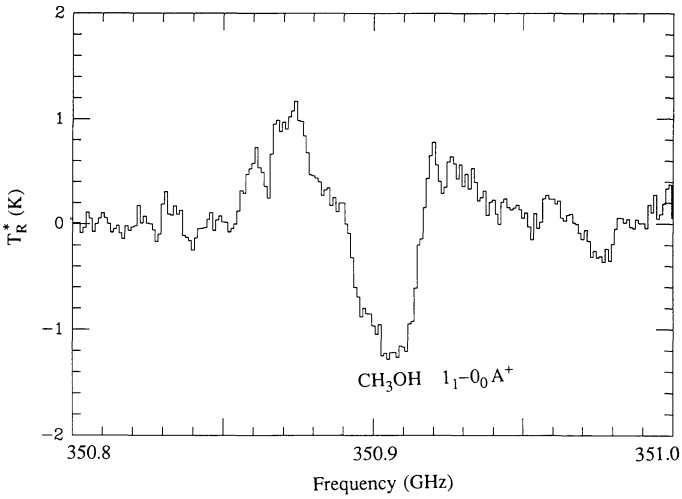

FIG. 7.—Spectrum of CH_3OH 1_1–0_0 A^+ transition, showing absorption shape similar to that seen in CN.

3.6. C_2H

The linear rotor C_2H is detected via the fine-structure doublet of $N = 4$–3. The higher frequency member of the doublet is blended with CH_3CN emission, so our analysis will be based solely on the lower frequency component. This in turn is a blend of two strong hyperfine components; our analysis is based on the sum of the intensities of those two components. Assuming excitation at 20 K, we derive a column density of 7.8×10^{14} cm^{-2}. Both low-frequency surveys (Cummins et al. 1986; Turner 1989, 1991) readily detected C_2H in Sgr B2, although neither gives abundance estimates for this species.

3.7. OCS *and* HC_3N

Heavier linear rotors have closely spaced transitions, so more than one feature can be seen in our frequency range. However, these do not sample a sufficient range of excitation energy to define a good rotation curve. The situation thus is similar to that for molecules seen in only a single transition, with the exception that as the moment of inertia gets larger, so do the excitation energies being sampled. We see the molecule OCS in a pair of transitions, $J = 28$–27 and $J = 29$–28, which involve energy levels about 250 K above the ground state. Populating these levels requires a temperature much greater

than the 11.6 K derived from Turner's fit to the low-frequency data. If we assume an excitation temperature of 200 K, we derive a column density of 1.3×10^{15} cm^{-2} for this higher excitation component, a value close to the 1.4×10^{15} cm^{-2} derived by Turner for the cool component. This is the first evidence for the presence of such a warm component of OCS in Sgr B2.

The molecule HC_3N is seen here in three high-J transitions: $J = 37$–36, $J = 38$–37, and $J = 39$–38. These again require a high-excitation component to provide the substantial population observed. Using data from low-excitation lines ($J = 8$–7 through $J = 12$–11), Turner (1991) derived an HC_3N column density of 3.1×10^{14} cm^{-2} and a rotational temperature of 13.6 K. A somewhat higher rotational temperature (36 K) and column density (4.9×10^{14} cm^{-2}) were obtained by Lis & Goldsmith (1991), also on the basis of low-energy data. These low-temperature components are unable to explain the intensities of the high-J lines seen here. Lis & Goldsmith have suggested that an even higher excitation component with an excitation temperature of order 70 K may be produced collisionally in a very dense core ($n_{H_2} \approx 10^7$ cm^{-3}). Adopting this excitation temperature, we require a column density of 2.6×10^{14} cm^{-2} to fit our high-J lines. In contrast, populations in vibrationally excited levels of HC_3N (Goldsmith et al. 1987; Lis & Goldsmith 1991; Turner 1991) are thought to be provided by radiative excitation.

3.8. CH_3CN *and* CH_3CCH

Methyl cyanide (CH_3CN) is weakly seen here in the $K = 0$ through $K = 3$ components of $J = 18$–17 and $J = 19$–18. These levels have excitation energies of about 200 K, significantly higher than for previously reported transitions of CH_3CN in this source. Our data are listed in Table 5 and plotted in rotation diagram form in Figure 8. For comparison we have also included the $K = 0$ data of Turner (1991) on the same plot. Turner employs a two-temperature model to describe the methyl cyanide excitation. In this method (cf. Cummins et al. 1983) a rotational temperature T_{rot} describes the excitation within the $K = 0$ ladder, and a kinetic temperature T_{kin} describes the relative excitation of different K ladders. While noting that Turner's data may fall somewhat low in comparison with ours owing to beam-dilution effects, it is clear that our high-J $K = 0$ data fall substantially above an extrapolation of his $K = 0$ line with its slope given by $T_{rot} = 9.8$ K. A full statistical equilibrium calculation will produce a more complex pattern of excitation (Loren & Mundy 1984; Sutton et al. 1986), but it is clear that for any collisional excitation model to support substantial population in $J = 19$ will require some regions with densities in excess of 10^6 cm^{-3}. It is also conceivable that population of these levels may be produced by radiative excitation via the v_8 vibrational state (Carroll & Goldsmith 1981). Further results on CH_3CN obtained using the JCMT will be presented in § 4.

Methyl acetylene (CH_3CCH) is also detected very weakly via the blended $K = 0$ and $K = 1$ components of $J = 20$–19. As with CH_3CN, these are high-energy transitions and demonstrate that this species must be present in a high-excitation component of the gas. Given the weakness of this feature, it is difficult to make any more quantitative statements about this molecule.

3.9. HNCO

Isocyanic acid (HNCO) is a highly prolate asymmetric top. For a structure of this sort, the rotational levels $J_{K_pK_o}$ with $K_p \geq 1$ all have relatively high excitation energies. The millimeter-wave spectrum of this molecule consists entirely of a-type transitions, since the b-type transitions all occur in the far-infrared (FIR). The excitation of HNCO in Sgr B2 has been discussed

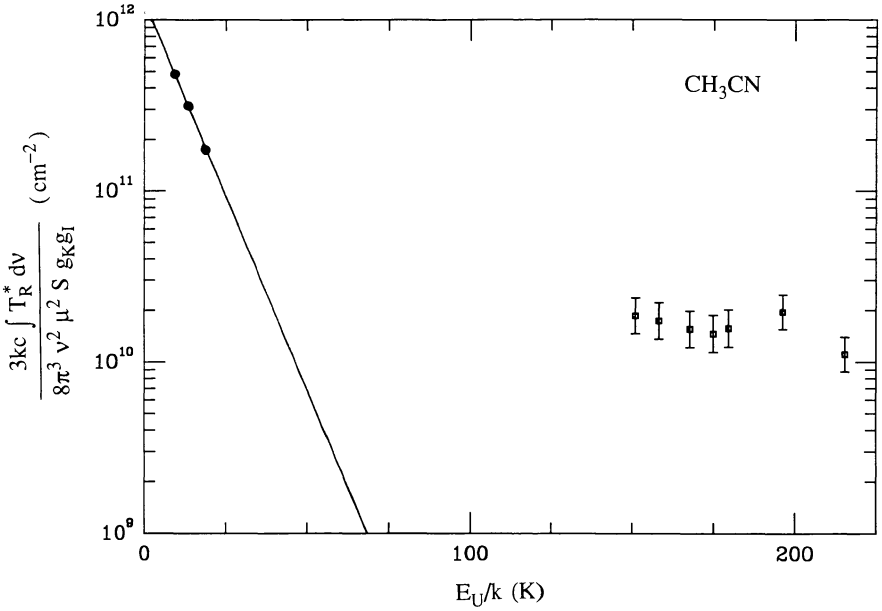

FIG. 8.—Rotation diagram for CH_3CN showing present data (*squares*), data from Turner (1991) (*filled circles*), and a linear fit to just the Turner data

in detail by Churchwell et al. (1986). They find that the *b*-type transitions are quite important determinants of the excitation, since they are extremely well coupled to the strong FIR field produced by the dust continuum. The *b*-type transitions are sufficiently rapid to equilibrate both the populations within K_p ladders and the populations of different K_p ladders.

The rotation curve of Churchwell et al. (1986) is in good agreement with the rotation curves of Cummins et al. (1986) (their fit incorporates the Cummins et al. data) and Turner (1991). All of these authors find a need for a two-component distribution at temperatures of about 10 and 70 K, with a total column density of about 2×10^{15} cm^{-2}. In Table 5 we list the four transitions of HNCO we have observed in Sgr B2(M). Our data show good agreement with these previous rotation curves. Since our results are from levels above 125 K, we are sensitive only to the warmer of the two components. Adopting the above value of 70 K for the rotation temperature of the warmer component, we derive a column density of 7.1×10^{14} cm^{-2}, in agreement with previous results. The majority of the HNCO is in the cooler component.

Churchwell et al. (1986) found HNCO in Sgr B2 to be distributed over a $3' \times 6'$ region centered somewhat north of Sgr B2(OH), based primarily on measurements of $7_{0,7}$–$6_{0,6}$. In contrast, Goldsmith et al. (1987) found that HNCO $5_{1,5}$–$4_{1,4}$ emission peaked on a rather compact source at the position of Sgr B2(N). This may be due to stronger radiative excitation in this part of the cloud; other radiatively excited transitions, such as those from vibrationally excited HC_3N, peak strongly in the north. However, Churchwell et al. also see spatially extended emission in the $10_{0,10}$–$9_{0,9}$ transition, which has an excitation energy comparable to the $5_{1,5}$ level. And the lines $15_{1,14}$–$14_{1,13}$, $16_{1,16}$–$15_{1,15}$, $16_{0,16}$–$15_{0,15}$, and $16_{1,15}$–$15_{1,14}$, all of which originate in even higher levels, are strongly present in Sgr B2(M). The reason for these different pictures of the high-excitation levels is not clear.

3.10. H_2CO *and* H_2CS

Formaldehyde (H_2CO) is seen in only a single line of $H_2{}^{12}CO$ and in two transitions of $H_2{}^{13}CO$. Assuming an excitation temperature of 20 K and an optically thin transition, the integrated intensity of the $H_2{}^{12}CO$ line yields a column density of about 4.7×10^{14} cm^{-2}. Two reasons suggest that this value may be too low. First, Turner's observations of the $1_{0,1}$–$0_{0,0}$ transition showed a self-absorbed profile, indicating large quantities of cold gas. The saturated behavior of that transition implied a lower limit to the column density of 8.1×10^{14} cm^{-2}. Second, our observations of $H_2{}^{13}CO$ suggest that the $H_2{}^{12}CO$ line is optically thick. Taking just the $H_2{}^{13}CO$ intensities and an isotopic ratio of $^{12}C/^{13}C = 28$, we derive an H_2CO column density of 1.9×10^{15} cm^{-2}. This result is relatively free of bias, since the $H_2{}^{13}CO$ lines are undoubtedly optically thin; however, the column density is somewhat uncertain because of the weakness of the $H_2{}^{13}CO$ lines.

Our data from H_2CS are sufficiently extensive to allow us to plot a rotation diagram, which is given in Figure 9. From this we derive an excitation temperature of 87 ± 19 K and a column density of $4.2 \pm 1.4 \times 10^{14}$ cm^{-2}. This temperature is larger than Turner's value of 48.8 K, although the uncertainties in the two quantities almost overlap. We should note that our value of the rotational temperature is largely determined by a single feature, the blended $K = 3$ doublet at 343410 MHz. Our column density is lower than Turner's value of 8.1×10^{14} cm^{-2}. This difference is due to the difference in rotational temperatures of our two fits. Our data sample higher-lying energy levels than those seen by Turner. The gas component we see is characterized by higher temperature and lower column density than that seen by Turner.

3.11. *Nondetections and Marginal Detections*

The high-frequency transitions of many molecules involve only high-lying energy levels. A typical situation is that of a

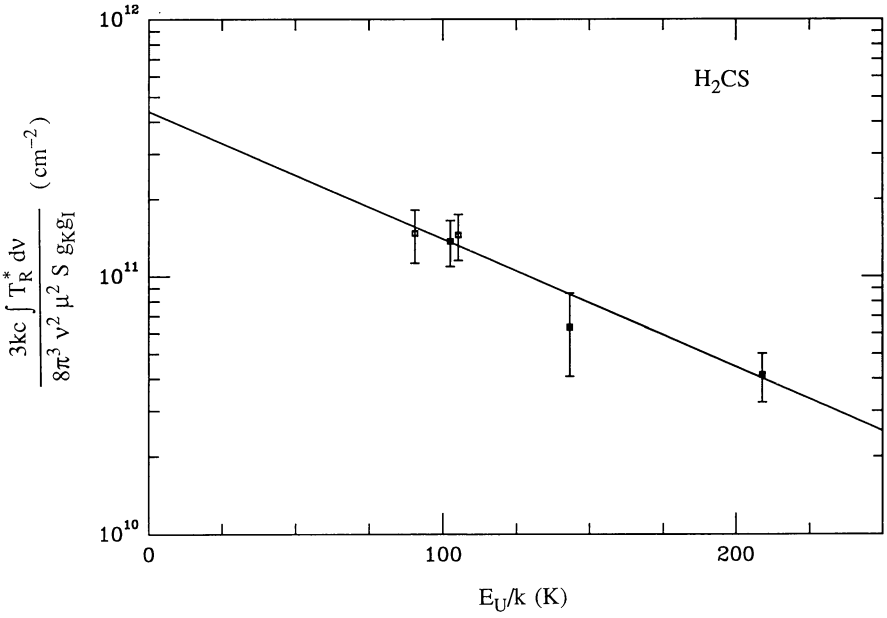

FIG. 9.—Rotation diagram for H_2CS

heavy molecule with only an *a*-dipole type spectrum, such as a linear molecule with a large moment of inertia. The high energy levels involved in these submillimeter transitions are often not populated in Sgr B2. Molecules seen at lower frequencies but which we fail to detect in this survey include SiS, HC_5N, HC_7N, C_4H, C_2S, SiC_2, and $HOCO^+$. Our upper limits for these species are consistent with the abundances deduced from the lower frequency surveys.

We also fail to detect several molecules with more modest energy levels which were detected in previous surveys. These include HCO, HNO, HCOOH, CH_2CN, $HCOOCH_3$, C_2H_3CN, and C_2H_5CN. Again, our upper limits are in agreement with these results.

Formamide (NH_2CHO) is illustrative of the problems inherent in observations of heavy rotors at high frequencies. Turner (1991) observed 18 transitions of this species, including numerous *a*-type transitions in the bands $J = 4$–3 and $J = 5$–4. He derived a fit to his data with a rotational temperature of 11.4 K and a column density of 2.1×10^{14} cm^{-2}. In our high-frequency band the only available *a*-type transitions are in the $J = 17$–16 and $J = 16$–15 bands. All of these transitions involve levels greater than 120 K above the ground state, which are not significantly populated at the rotational temperature seen by Turner. The best candidates for detection are three *b*-type transitions: $8_{2,7}$–$7_{1,6}$, $9_{2,8}$–$8_{1,7}$, and $7_{2,5}$–$6_{1,6}$, which involve only low-lying levels. Taking the rotation curve of Turner, we would predict integrated intensities of about 0.2 K km s^{-1} for these lines, which is over an order of magnitude weaker than our detection limit. Thus our failure to detect formamide is consistent with its detection at lower frequencies, even if we postulate a rather higher column density in the smaller, high-frequency beam.

The situation for acetaldehyde (CH_3CHO) is similar to that for formamide, with the additional complication that frequencies for the high-J *a*-type transitions are currently not well predicted. We do not detect any of the lower energy *b*-type transitions for which frequencies are available. Our limits are consistent with Turner's rotational temperature of 9.4 K and column density of 2.2×10^{14} cm^{-2}.

Transition frequencies for dimethyl ether (CH_3OCH_3) have recently been made available by Herbst (1990), although line strengths have not yet been tabulated for transitions in our frequency band. We do not clearly detect any dimethyl ether transitions in the CSO data. Based on estimated line strengths, we conclude that our limits are marginally consistent with the column densities derived by Turner. Dimethyl ether will be discussed more fully in § 4.4 below.

Cyclopropenylidene (C_3H_2) suffers in these observations from being a comparatively low-abundance species with low rotational temperature, making it difficult to detect in our band. We appear to have marginally detected it in two transitions, as listed in Table 5. The remaining transitions in our band unfortunately fall in relatively noisy regions of the spectrum. We derive a rotational temperature of 27.0 ± 5.3 K and a column density of $8.6 \pm 4.5 \times 10^{13}$ cm^{-2}, consistent with Turner's values of 15^{+16}_{-5} K and $5.0^{+3.5}_{-2.0} \times 10^{13}$ cm^{-2}. Our detection of C_3H_2 is supported by detection of several other lines in the JCMT data which will be discussed in § 4.

We may have obtained a marginal detection of ketene (CH_2CO) via a single ortho transition ($17_{1,17}$–$16_{1,16}$). Unfortunately, the frequency of this line is in near-coincidence with what should be the strongest ethanol transition in our survey. The other $K = 1$ transition ($17_{1,16}$–$16_{1,15}$) of ketene is in a crowded region of the spectrum and is not clearly seen. We also do not see the lowest-lying para transition ($17_{0,17}$–$16_{0,16}$). Assuming that the entire intensity of the line we do see can be attributed to ketene and assuming Turner's rotational temperature of 70.5 K, we estimate a column density of $3.9 \pm 1.7 \times 10^{14}$ cm^{-2}, marginally consistent with Turner's $7.5^{+2.9}_{-2.0} \times 10^{14}$ cm^{-2}.

Ethanol (C_2H_5OH) has a large moment of inertia and thus has many transitions in our band, all of which are weak, in part because of the large partition function. Based on Turner's fit with a rotational temperature of 35.7 K and a column density of 1.3×10^{15} cm^{-2}, we would only expect a single (*K*-doubled) transition to be detectable in our data set. Unfortunately, this is coincident in frequency with a ketene line, as discussed above. As with ketene, we do not know what fraction of the observed intensity to attribute to ethanol.

Methanimine (CH_2NH) is seen weakly in emission in two transitions. Taking the stronger of these and assuming a rotational temperature of 20 K, we derive a column density of 4.5×10^{14} cm^{-2}, reasonably consistent with Turner's value of 2×10^{14} cm^{-2}. A third, lower-lying transition of CH_2NH is seen in absorption. This may simply represent a second cold component of gas in the foreground. The issue of population distribution in the lower levels of CH_2NH is discussed briefly by Turner (1991).

We do not convincingly see any transitions of cyanamide (NH_2CN), for which all lines in our band originate in levels of high energy. Our upper limits are inconsistent with Turner's fit using a rotational temperature of 91.2 K and a column density of 1.1×10^{14} cm^{-2}. However, our data are consistent with Turner's alternative solution (in which he omits one data point) which gives a temperature of 29 K and a column density of 2.9×10^{13} cm^{-2}. This latter solution is also more consistent with the results of Cummins et al. (1986).

4. MEASUREMENTS COMPARING SAGITTARIUS B2(N) AND SAGITTARIUS B2(M)

In this section we discuss measurements made with the JCMT which directly compare molecular line emission from Sgr B2(M) and Sgr B2(N). The JCMT observations consist of pairs of spectra from these two sources at a variety of local oscillator settings. Generally speaking, the JCMT data have sensitivity comparable to or somewhat better than that of the CSO data, although the JCMT data have very limited spectral coverage. Because redundant frequency coverage was not obtained, it was not possible to deconvolve the overlapping sidebands. The JCMT data are presented as double-sideband spectra. Line identifications have been made and sideband ambiguities have been resolved, where possible, by reference to the CSO data.

Our beam at the JCMT was quite small ($\sim 14''$), and the northern source, in particular, is known to be quite compact. Consequently, we preceded our observations by pointing checks using the CS $J = 7$–6 line. The CS source in Sgr B2(N) was found to be compact ($\lesssim 20''$) and was centered on our nominal coordinates within a pointing uncertainty of about $3''$.

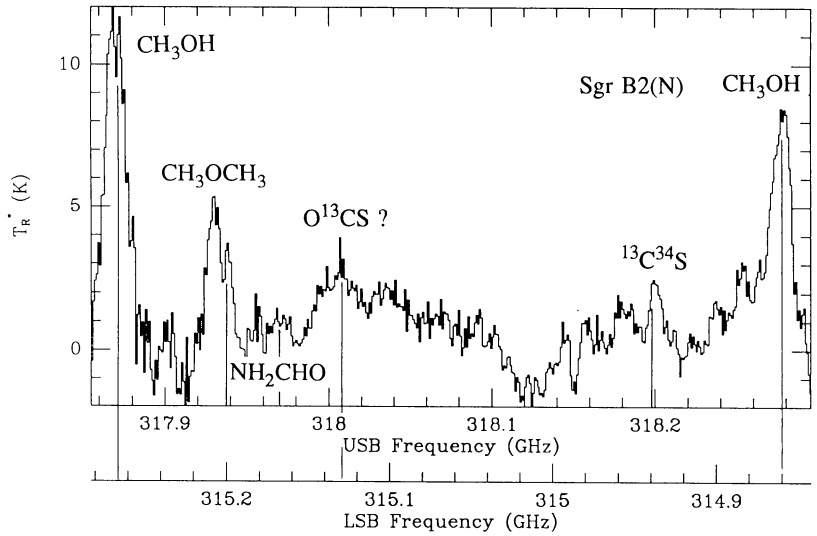

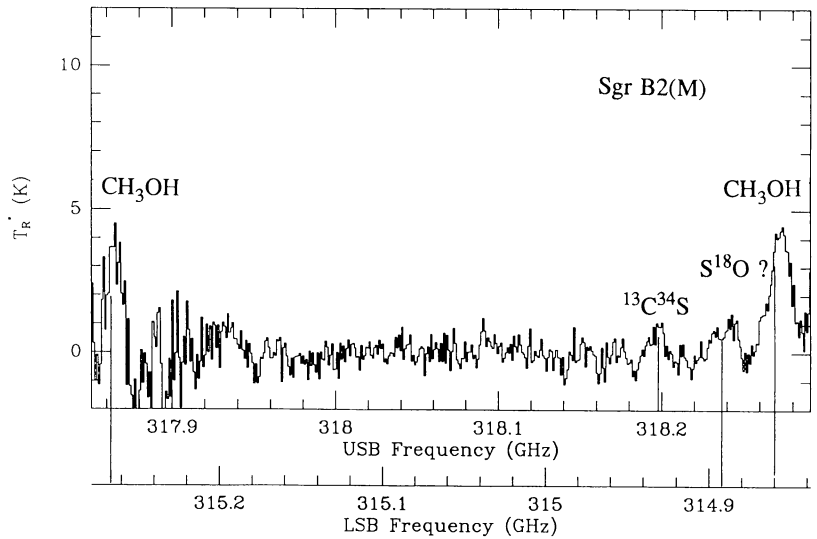

FIG. 10*a*

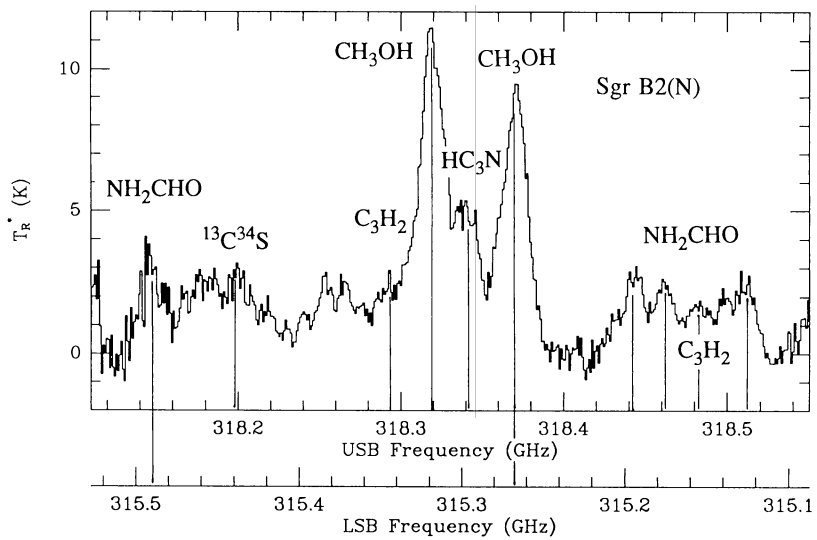

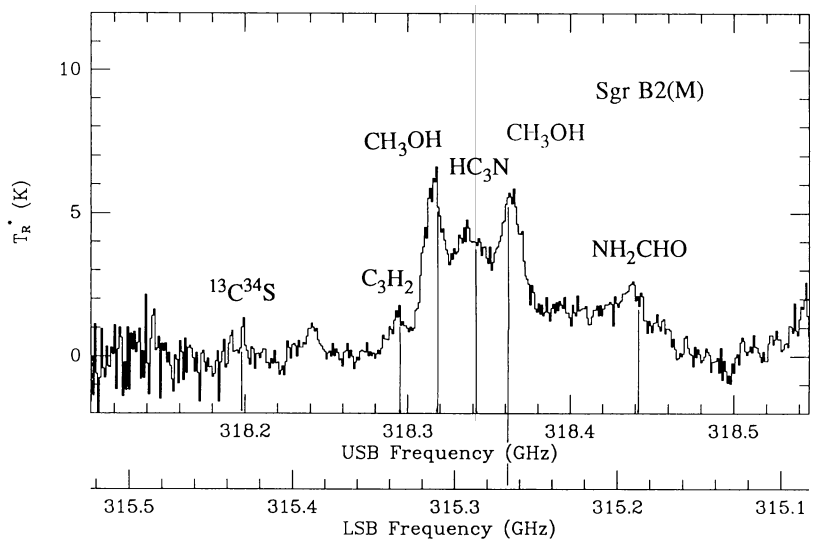

FIG. 10*b*

FIG. 10.—Double-sideband spectra of Sgr B2(M) and Sgr B2(N) obtained using the JCMT. Rest-frequency scales assume a v_{lsr} of 61 km s^{-1} for Sgr B2(M) and 65 km s^{-1} for Sgr B2(N). Notice for Sgr B2(N) the large density of lines and the redshifted absorption cores seen in (*f*) H^{13}CN, (*g*, *h*) CS, and (*i*) H^{13}CO$^+$.

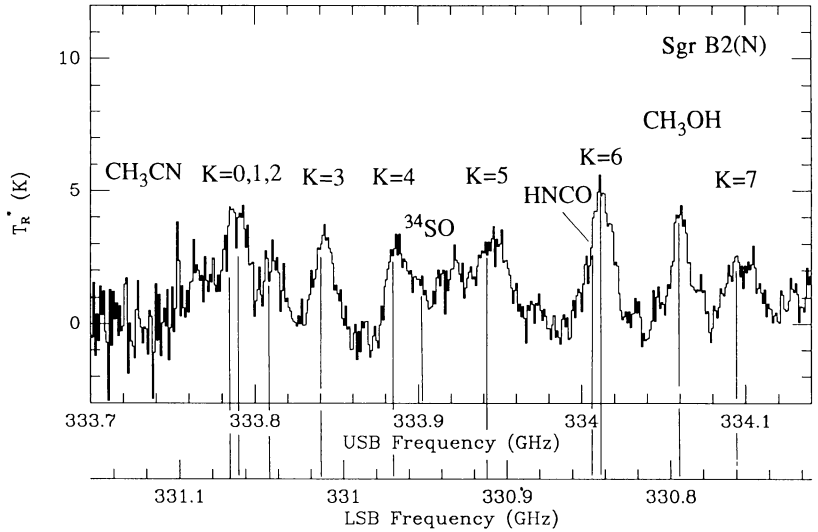

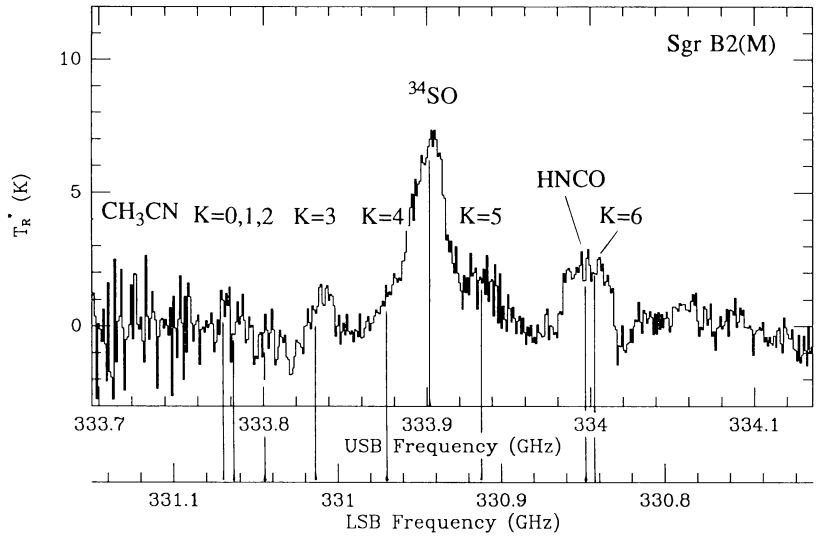

FIG. 10*c*

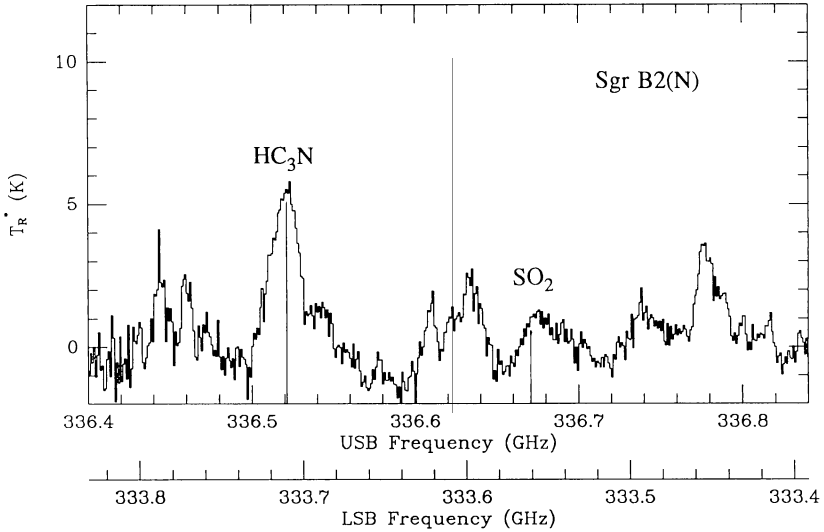

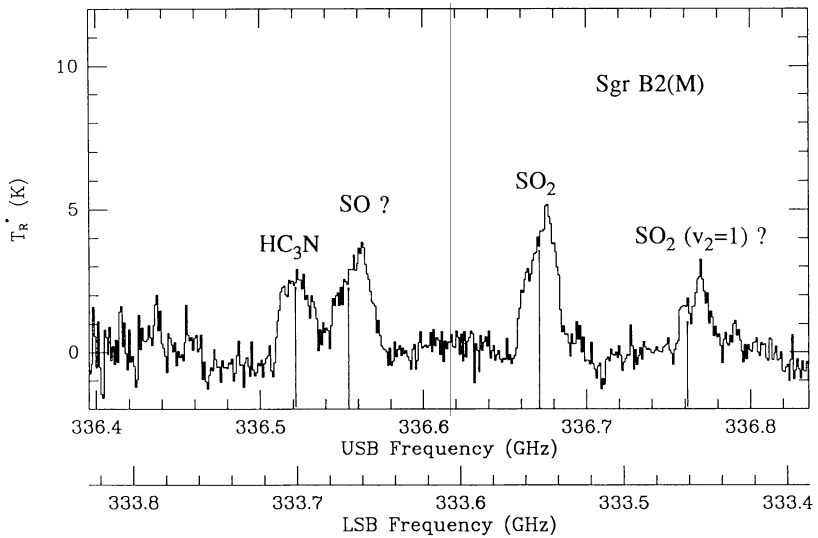

FIG. 10*d*

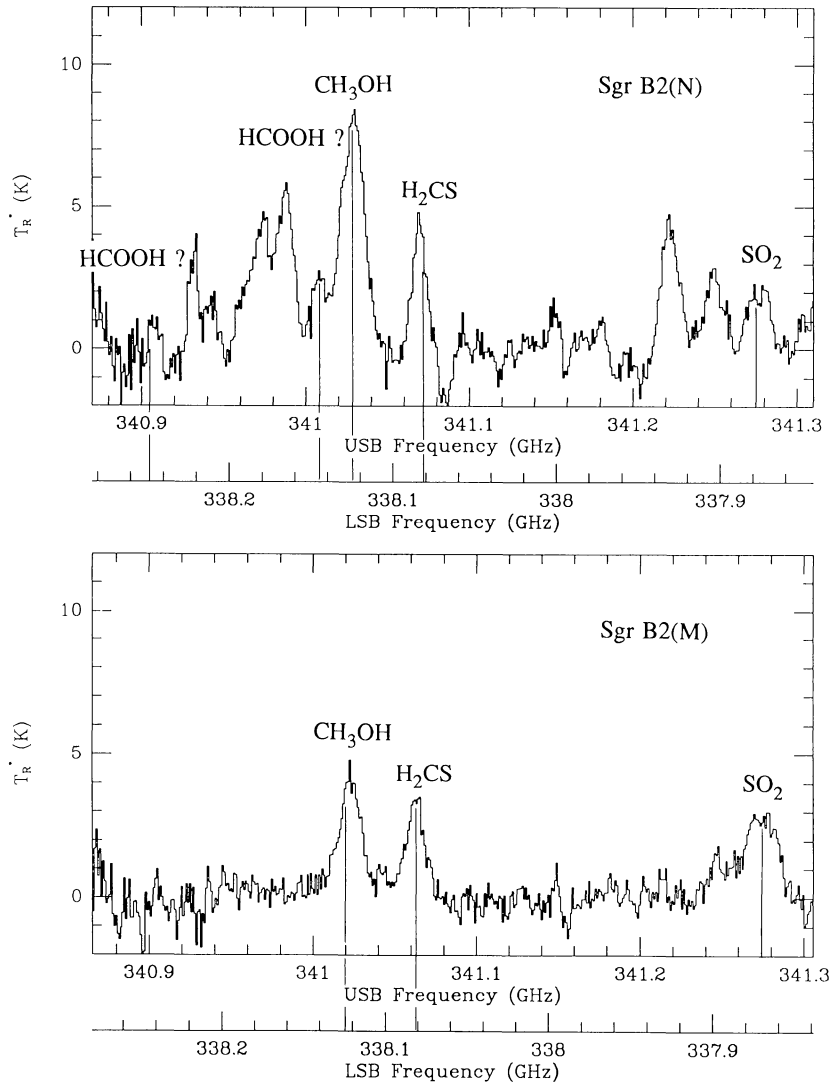

FIG. 10*e*

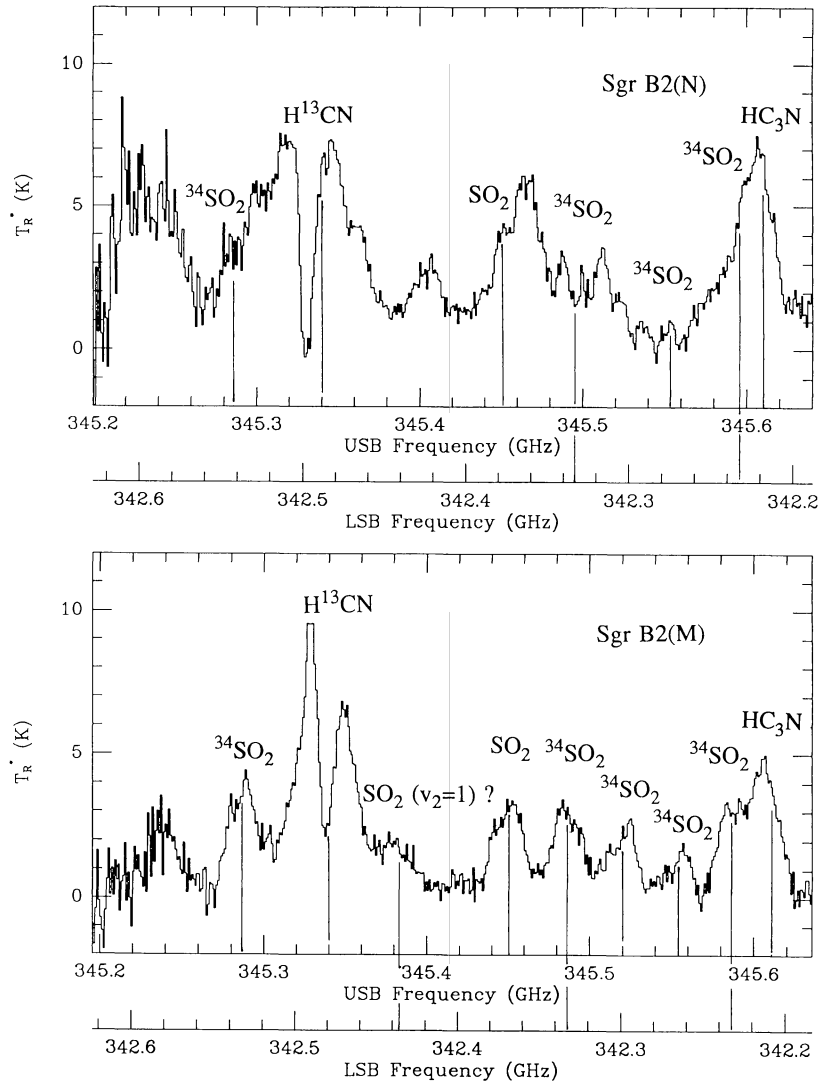

FIG. 10*f*

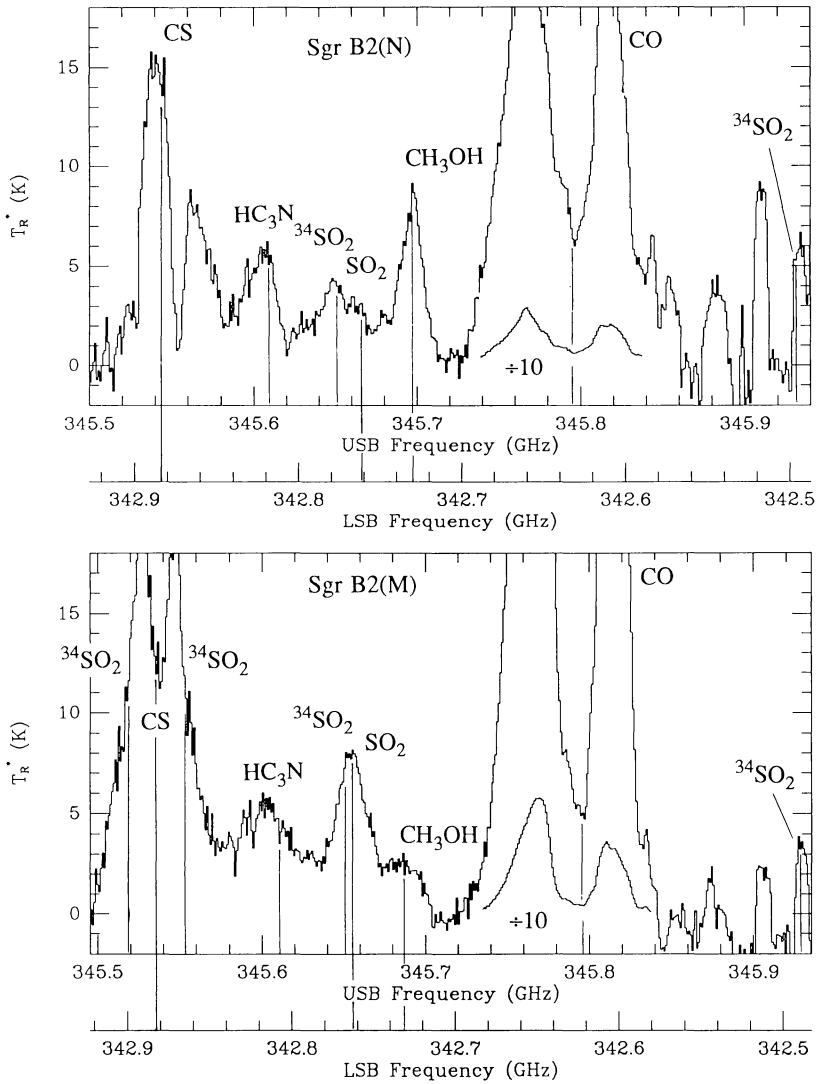

FIG. 10*g*

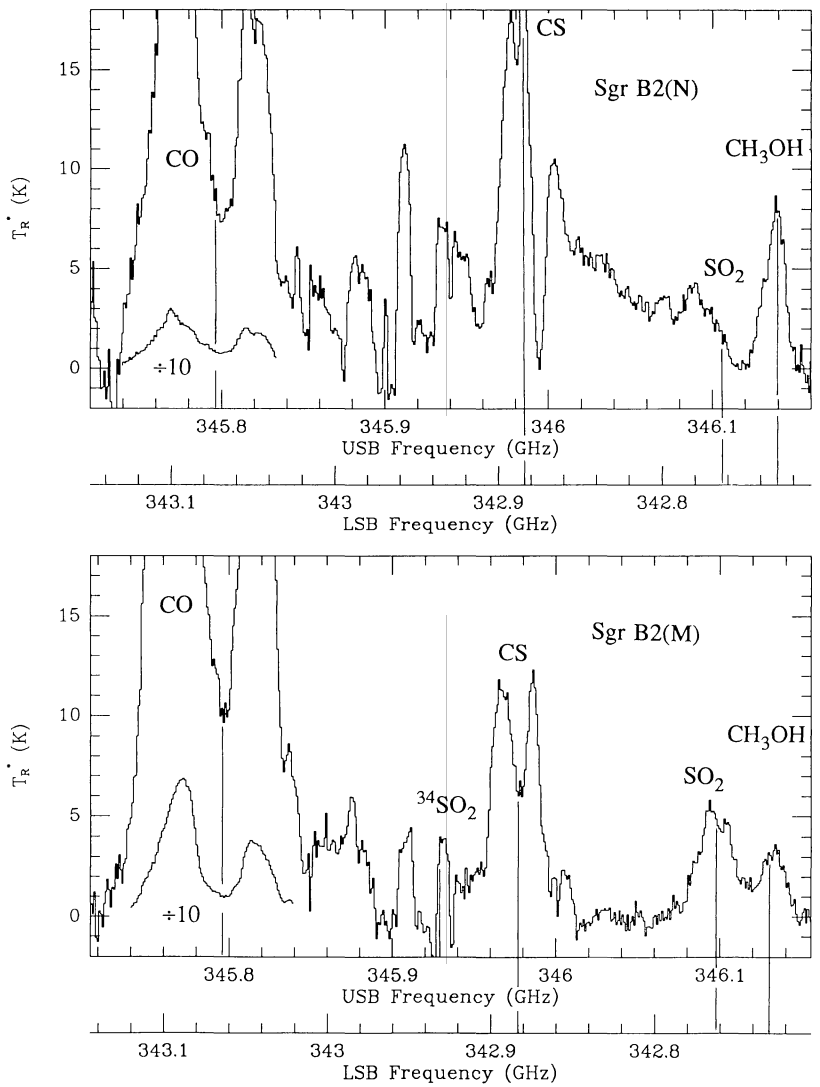

FIG. 10*h*

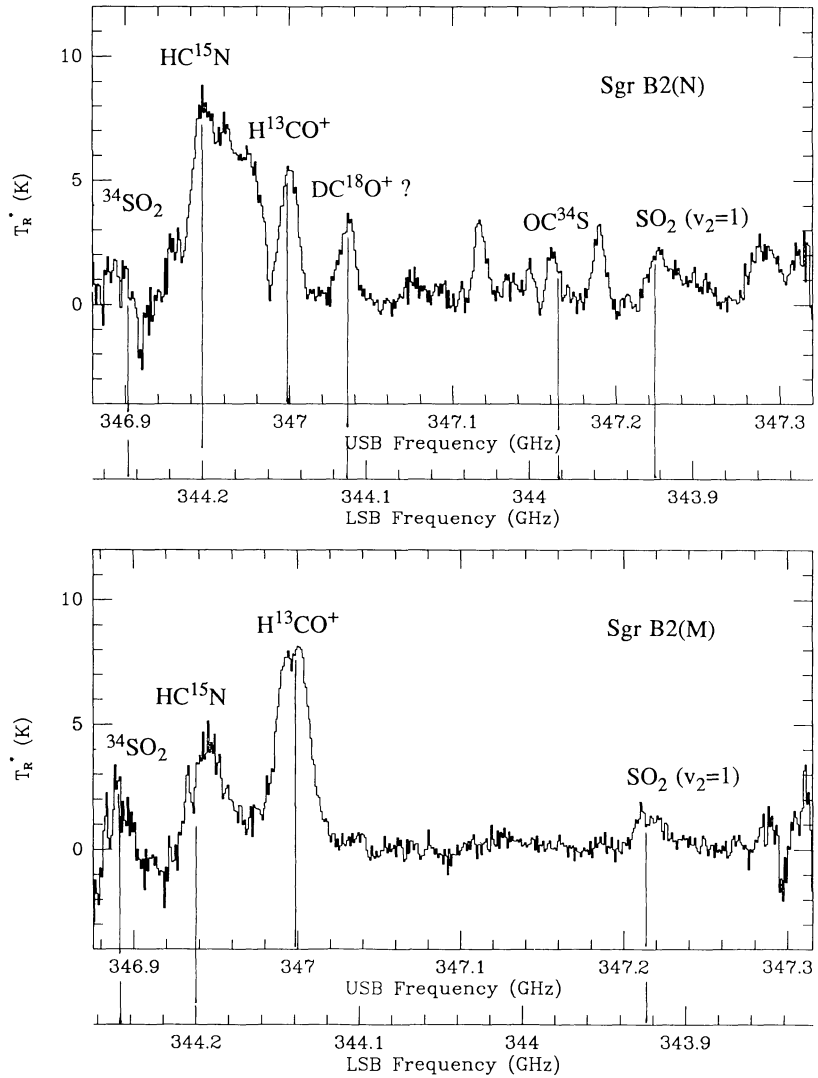

FIG. 10*i*

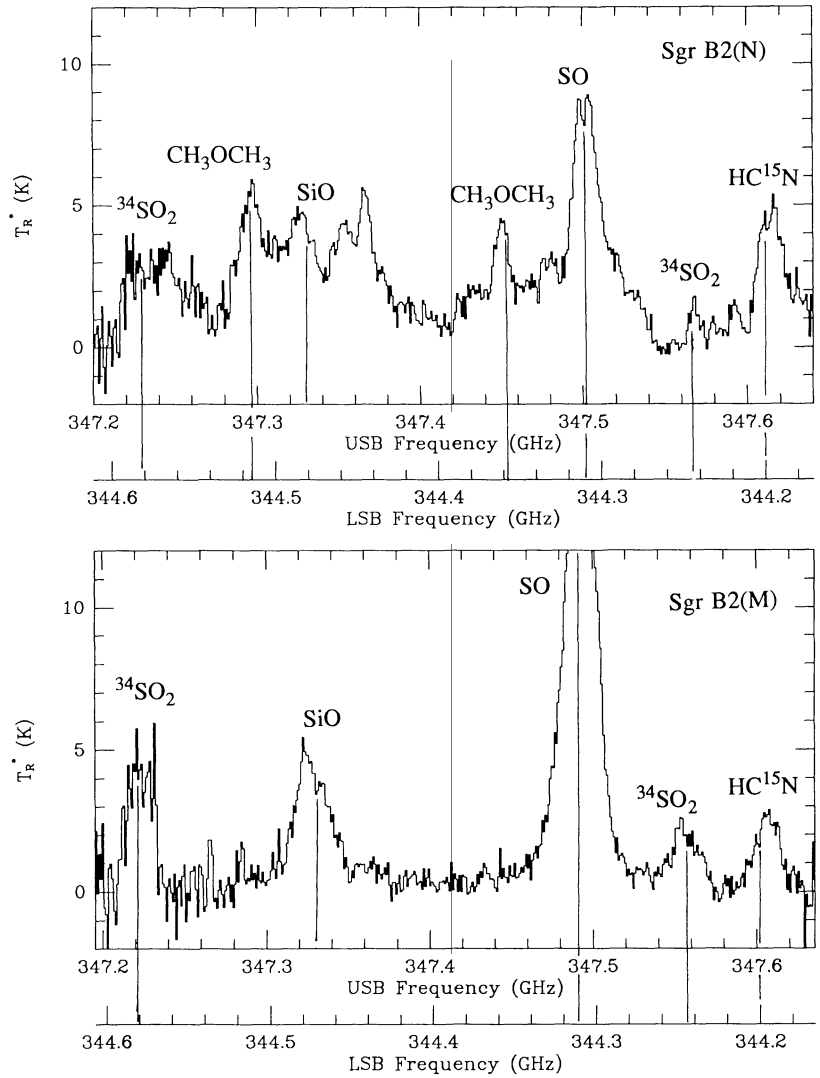

FIG. 10*j*

In Sgr B2(M) the peak CS emission again occurred near our nominal position, but there was significant extended emission, particularly to the north and west, generally similar to the distribution of SO as seen by Goldsmith et al. (1987).

In Figure 10 we present 10 sets of double-sideband (DSB) spectra from the JCMT comparing Sgr B2(N) and Sgr B2(M). The rest-frequency scales for the two sources have been prepared assuming a v_{lsr} of 65 km s^{-1} for Sgr B2(N) and 61 km s^{-1} for Sgr B2(M). The spectra for Sgr B2(N) are clearly very crowded. There are numerous currently unidentified lines, for most of which we are unable to provide sideband assignments because of the heavy blending and the fact that most have been observed only at single local oscillator settings. Line shapes are also very complex in Sgr B2(N), making it difficult to distinguish between the case of adjacent emission features and that of a broad self-reversed profile. The identified features from Figure 10 are summarized in Table 6.

These observations reveal a number of striking differences between Sgr B2(M) and Sgr B2(N). These differences can be grouped into several broad categories. It is clear that for most species Sgr B2(N) has a larger column density than Sgr B2(M), as indicated by the presence of a number of rare isotopic forms and other species not detected in Sgr B2(M). This is also seen in the line profiles of the more heavily saturated transitions. In contrast, the molecules SO and SO_2 are very underabundant in Sgr B2(N) relative to most other species. Finally, there are differences in excitation between the two sources, generally corresponding to higher excitation in Sgr B2(N). There have been previous indications of each of these phenomena, although these observations provide important new detail. In the sections which follow we will discuss the results seen in a variety of molecules and the implied differences between Sgr B2(M) and Sgr B2(N).

4.1. OCS, CS, *and* HCO^+

A variety of lines appearing in Sgr B2(N) but not in Sgr B2(M) can be attributed to rare isotopic forms. Any of these could be a simple misidentification. But the number of such occurrences suggests that there is a sufficiently high column density associated with Sgr B2(N) to allow these rarer species to be observable. The best illustration of this effect is given by Figure 10*i*. In this set of data, emission is seen from Sgr B2(N) at a number of frequencies where little or no emission can be seen from Sgr B2(M). A number of these features are currently unidentified, although there are two which we have tentatively identified as $OC^{34}S$ and $DC^{18}O^+$. The observations in Figures 10*a* and 10*b* suggest the presence of $^{13}C^{34}S$. These identifications are tentative, since they are single lines of each species and because the spectrum is clearly quite crowded. However, we will argue that these identifications are plausible in terms of their integrated intensities.

Although we did not have sufficient data to construct a full rotation diagram, we clearly detected OCS emission in our CSO data from Sgr B2(M) at an integrated intensity level ($\int T_R^* dv$) of about 16 K km s^{-1}. These lines of the dominant isotope were not reobserved using the JCMT; however, we would expect them to be brighter ($\gtrsim$23 K km s^{-1}) because of the smaller beam size and higher main-beam efficiency obtained on the JCMT. For observing $OC^{34}S$ in Sgr B2(M), this gain would be more than offset by the lower abundance of the isotopic form (assuming $^{32}S/^{34}S = 18$). And indeed we do not appear to see $OC^{34}S$ in Sgr B2(M). On the other hand, it is more likely that $OC^{34}S$ would be observable in Sgr B2(N) given the fact that the OCS $J = 9$–8 emission is known to peak around the northern position (Goldsmith et al. 1987). The degree of enhancement in integrated intensity is difficult to estimate, since in our JCMT observations we are dealing with high-energy lines ($\sim$200 K). But since Sgr B2(N) is thought to be more highly excited than Sgr B2(M), the enhancement of the former over the latter should be even greater than that seen by Goldsmith et al. Given these factors, the detection of $OC^{34}S$ at the level seen in Figure 10*i* is quite plausible. The spectrum of Sgr B2(N) in Figure 10*a* indicates that we also may have detected $O^{13}CS$.

A second rare species seen in both Sgr B2(M) and Sgr B2(N) is the doubly isotopic-substituted form $^{13}C^{34}S$. Our results are shown in Figures 10*a* and 10*b* and are listed in Table 6. The main isotopic ($^{12}C^{32}S$) $J = 7$–6 line has roughly equal integrated intensities in the two sources and is surely saturated, as was indicated by the CSO data. Line profiles in both sources indicate substantial self-reversal (Figs. 10*g* and 10*h*). The detection of $^{13}C^{34}S$ is plausible for isotopic ratios of $^{12}C/^{13}C \approx 28$ and $^{32}S/^{34}S \approx 18$ only if the main line is quite optically thick. We appear to see $^{13}C^{34}S$ in both Sgr B2(M) and Sgr B2(N), although with somewhat higher intensity in the latter.

A third rare species we *may* have observed is $DC^{18}O^+$. It is difficult to predict deuterium fractionation accurately (cf. Millar, Bennett, & Herbst 1989), although it is clear that at least under some circumstances the abundance of the deuterated form can approach that of the nondeuterated molecule (Turner 1990). We know that we have observed $H^{13}CO^+$ and $HC^{18}O^+$ in the CSO survey data on Sgr B2(M), and $H^{13}CO^+$ is also clearly present in Figure 10*i* in both Sgr B2(M) and Sgr B2(N). The line shape in Sgr B2(N) is quite complex, in part because of blending with $HC^{15}N$, but it appears that $H^{13}CO^+$ is strongly self-reversed. The strong redshifted absorption core is a feature also seen in CS (Figs. 10*g* and 10*h*) and $H^{13}CN$ (Fig. 10*f*). The apparently high optical depth suggests that identification of $DC^{18}O^+$ in Sgr B2(N) may be correct. Given the difference in the $H^{13}CO^+$ profiles between Sgr B2(N) and Sgr B2(M), it also seems likely that $DC^{18}O^+$ would not be seen in Sgr B2(M).

4.2. SO *and* SO_2

Goldsmith et al. (1987) clearly showed that sulfur monoxide (SO) was concentrated around Sgr B2(M). This can be seen in Figure 10*j*, where the 8_8–7_7 line of SO is clearly stronger in Sgr B2(M) than in Sgr B2(N), even though this line is somewhat saturated. A line at 336553 MHz was tentatively identified as SO 11_{10}–10_{10} on the basis of the CSO data. This identification is supported here by the observation that it has a greater intensity in Sgr B2(M) than in Sgr B2(N), as shown in Figure 10*d* and Table 6. We have also observed two isotopic SO lines. The 8_7–7_6 line of ^{34}SO is observed in Sgr B2(M) and probably in Sgr B2(N), the line in Sgr B2(N) being about 10 times weaker (Fig. 10*c*). We also appear to

TABLE 6

LINES OBSERVED IN SAGITTARIUS B2(M) AND SAGITTARIUS B2(N) USING THE JCMT

Frequency (MHz)	Species	Transition	E_L (cm^{-1})	$\int T_R^* dv$ (M) (K km s^{-1})	$\int T_R^* dv$ (N) (K km s^{-1})	Notes
314859.6	CH_3OH	$7_1A^- - 7_0A^+$	45.2	57.	166.	
314891.7	$S^{18}O$?	$8_7 - 7_6$	42.3	21.	...	a
315128.8	$O^{13}CS$?	26-25	131.4	< 10.	?	a
315266.8	CH_3OH	$6_2 - 5_1$ E	38.7	59.	155.	
315489.3	NH_2CHO	$15_{2,14} - 14_{2,13}$	82.3	< 15.	36.	
317937.7	CH_3OCH_3	$18_{1,17} - 17_{2,16}$	110.5	< 15.	32.	b
317970.5	NH_2CHO	$12_{3,10} - 12_{2,11}$	63.3	< 10.	14.	
318197.7	$^{13}C^{34}S$	7-6	31.8	10.	25.	
318294.3	C_3H_2	$9_{0,9} - 8_{1,8}$	44.7	} 11.	13.	
318294.3	C_3H_2	$9_{1,9} - 8_{0,8}$	44.7			
318318.8	CH_3OH	$8_1A^- - 8_0A^+$	58.1	78.	228.	
318341.4	HC_3N	35-34	180.5	49.	88.	
318441.6	NH_2CHO	$15_{10,5} - 14_{10,4}$	281.1	} 14.	41.	
318441.6	NH_2CHO	$15_{10,6} - 14_{10,5}$	281.1			
318442.2	NH_2CHO	$15_{9,6} - 14_{9,5}$	241.9			
318442.2	NH_2CHO	$15_{9,7} - 14_{9,6}$	241.9			
318462.2	NH_2CHO	$15_{8,8} - 14_{8,7}$	206.7	} < 10.	29.	
318462.2	NH_2CHO	$15_{8,7} - 14_{8,6}$	206.7			
318482.2	C_3H_2	$8_{1,7} - 7_{2,6}$	42.5	} < 10.	23.	
318482.2	C_3H_2	$8_{2,7} - 7_{1,6}$	42.5			
318511.7	NH_2CHO	$15_{7,9} - 14_{7,8}$	175.7	} < 10.	31.	
318511.7	NH_2CHO	$15_{7,8} - 14_{7,7}$	175.7			
330760.2	CH_3CN	$18_7 - 17_7$	337.5	< 10.	35.	c,d,e
330793.9	CH_3OH	$8_{-3} - 9_{-2}$ E	90.5	< 10.	53.	
330842.6	CH_3CN	$18_6 - 17_6$	272.9	< 25.	60.	f
330848.8	HNCO	$15_{1,14} - 14_{1,13}$	107.3	50.	17.	f
330912.5	CH_3CN	$18_5 - 17_5$	218.2	15.	50.	e
330969.6	CH_3CN	$18_4 - 17_4$	173.4	15.	45.	e
331014.1	CH_3CN	$18_3 - 17_3$	138.6	30.	55.	
331045.9	CH_3CN	$18_2 - 17_2$	113.8	10.	37.	
331065.0	CH_3CN	$18_1 - 17_1$	98.9	13.	45.	e
331071.3	CH_3CN	$18_0 - 17_0$	93.9	13.	45.	e
333901.0	^{34}SO	$8_7 - 7_6$	44.4	169.	15.	e
336521.0	HC_3N	37-36	202.1	56.	110.	
336553.3	SO (?)	$11_{10} - 10_{10}$	88.1	75.	6.	d,g
336669.6	SO_2	$16_{7,9} - 17_{6,12}$	159.1	85.	38.	
336760.7	SO_2 (v_2=1) ?	$20_{1,19} - 19_{2,18}$	650.	8.	< 10.	
338080.8	H_2CS	$10_{1,10} - 9_{1,9}$	59.9	46.	50.	
338124.5	CH_3OH	$7_0 - 6_0$ E	42.8	46.	134.	
338143.7	HCOOH ?	$15_{4,12} - 14_{4,11}$	114.2	< 10.	7.	
338204.0	C_3H_2	$5_{5,1} - 4_{4,0}$	22.6	< 10.	< 15.	
338248.7	HCOOH ?	$15_{4,11} - 14_{4,10}$	114.2	< 10.	20.	
341275.5	SO_2	$21_{8,14} - 22_{7,15}$	245.2	64.	49.	
342231.7	$^{34}SO_2$	$20_{1,19} - 19_{2,18}$	126.4	53.	...	a
342332.1	$^{34}SO_2$	$12_{4,8} - 12_{3,9}$	64.7	49.	...	a
342435.9	SO_2 (v_2=1) ?	$23_{3,21} - 23_{2,22}$	704.	15.	< 10.	
342729.8	CH_3OH	$13_1A^- - 13_0A^+$	146.7	46.	103.	
342761.6	SO_2	$34_{3,31} - 34_{2,32}$	393.0	83.	33.	
342882.9	CS	7-6	34.3	...	...	h,i
343923.8	SO_2 (v_2=1)	$24_{2,22} - 23_{3,21}$	715.	22.	39.	
343983.3	$OC^{34}S$	29-28	160.7	< 5.	13.	
344112.8	$DC^{18}O^+$?	5-4	23.0	< 5.	30.	
344200.3	$HC^{15}N$	4-3	17.2	60.	130.	
344245.4	$^{34}SO_2$	$10_{4,6} - 10_{3,7}$	49.9	39.	22.	
344310.6	SO	$8_8 - 7_7$	49.3	340.	178.	
344358.0	CH_3OCH_3	$19_{1,19} - 18_{0,18}$	116.2	< 10.	23.	d
344515.	CH_3OCH_3	$11_{3,9} - 10_{2,8}$	50.6	5. ?	65.	
344581.1	$^{34}SO_2$	$19_{1,19} - 18_{0,18}$	104.9	78.	31.	
345285.7	$^{34}SO_2$	$9_{4,6} - 9_{3,7}$	43.5	70.	28.	
345339.8	$H^{13}CN$	4-3	17.3	...	...	h,i
345449.0	SO_2	$26_{9,17} - 27_{8,20}$	350.6	50.	25.	
345519.8	$^{34}SO_2$	$7_{4,4} - 7_{3,5}$	32.7	41.	...	a
345553.2	$^{34}SO_2$	$6_{4,2} - 6_{3,3}$	28.2	15.	7.	
345610.1	HC_3N	38-37	213.3	39.	107.	
345651.4	$^{34}SO_2$	$5_{4,2} - 5_{3,3}$	24.4	26.	18.	
345796.0	CO	3-2	11.2	...	...	h
345929.3	$^{34}SO_2$	$17_{4,14} - 17_{3,15}$	112.5	23.	...	a
346998.5	$H^{13}CO^+$	4-3	17.4	146.	...	h,i
347330.6	SiO	8-7	40.6	85.	80.	e

[a] Spectrum confused in (N), difficult to estimate intensity.
[b] Noisy region of spectrum.
[c] Breadth of line indicates possible blend.
[d] Frequency shift indicates possible blend.
[e] Integrated intensity in (N) is estimated.
[f] See text for discussion of how integrated intensity has been apportioned between HNCO and CH_3CN.
[g] Identification uncertain.
[h] Strongly self-reversed.
[i] (N) spectrum shows redshifted absorption core at v_{lsr} = 75 km s^{-1}.

have detected $S^{18}O$ 8_7–7_6 in Sgr B2(M) (Fig. 10*a*), although its intensity relative to ^{34}SO is somewhat greater than would be expected for $^{32}S/^{34}S = 18$ and $^{16}O/^{18}O = 476$.

A similar pattern is seen in sulfur dioxide, SO_2. This can be seen easily in the two $^{34}SO_2$ lines in Figure 10*j*, which are clearly stronger in Sgr B2(M). This is also seen in a number of other SO_2 and $^{34}SO_2$ lines. A rotation diagram for these data is shown in Figure 11. The relative strengths of SO_2 and $^{34}SO_2$ are similar to that shown in Figure 3, suggesting that both sources may be somewhat optically thick. If so, the higher integrated intensities observed from Sgr B2(M) may reflect a larger beam filling factor at the middle position.

4.3. *Methyl Cyanide* (CH_3CN) *and Methanol* (CH_3OH)

In the CSO survey data from Sgr B2(M), we observed methyl cyanide only out to $K = 3$, in both the $J = 18$–17 and $J = 19$–18 bands. The JCMT observations of Sgr B2(M) in $J = 18$–17 (Fig. 10*c*) reveal in addition the possible presence of $K = 4$ and $K = 5$ components, visible as shoulders on a ^{34}SO line in the opposite sideband. The detection of these weaker features is possible due to the smaller beam size and higher beam efficiency we obtained during the JCMT observations. In Sgr B2(N) we observe stronger emission lines in all of the components, enabling us to see out to $K = 7$. In principle, because of the crowding of the spectrum and because these are DSB observations, one or more of these lines may be misidentified. However, we believe that the overall pattern is quite convincing. The $K = 6$ line of CH_3CN is blended with an HNCO line. We have attempted to estimate the contribution of each species to the total integrated intensity, as will be discussed below in § 4.4.

A rotation diagram for the JCMT CH_3CN data is shown in Figure 12 based on the integrated intensities given in Table 6. The rotation curve is extremely flat, similar to the curve for the CSO data (Fig. 8) but extending to much higher energy. This behavior may be attributed to extreme saturation or to a peculiar pattern of excitation. Saturation seems unlikely because of the general weakness of the features and the fact that the lines are significantly stronger in Sgr B2(N) than in Sgr B2(M). If saturation is not present, the slope of the rotation curve would imply an excitation temperature in excess of 1000 K for these high levels, clearly very different than the 9.8 K rotation temperature of the lower levels (Turner 1991). As discussed in § 3.8, it is clear that the excitation pattern is not simple. It is also clear that some fraction of the CH_3CN in both Sgr B2(M) and Sgr B2(N) is excited to very high energies. Given the obvious breakdown of LTE and the fact that the majority of the CH_3CN is in cooler gas not sampled here, it seems inadvisable to attempt to use Figure 12 to derive CH_3CN column densities.

The differences in methanol emission between Sgr B2(N) and Sgr B2(M) provide a somewhat similar picture. A variety of methanol transitions are visible in Figure 10 and listed in Table 6. All give higher integrated intensities in Sgr B2(N), suggesting the presence of a higher column density of methanol in Sgr B2(N) than Sgr B2(M). The intensity ratio is of order 3, but is smallest for those lines with the highest intensities, indicating some line saturation in the northern source. This saturation is sufficient to mask any obvious dependence on excitation energy in the present data set, which is comprised mostly of moderate excitation (100 K) lines.

4.4. CH_3OCH_3, NH_2CHO, C_3H_2, *and* HNCO

The species dimethyl ether (CH_3OCH_3) was not convincingly seen in the CSO survey data, although weak features could be seen at a few of the expected frequencies. In the JCMT data we have detected three transitions of dimethyl ether, based on frequencies of Herbst (1990). These are shown in Figures 10*a* and 10*j* and are listed in Table 6. In all cases the emission is strong in the northern source (N) and weak or absent in the middle source (M). We have analyzed the data by ignoring the torsional splittings, which in the worst case span 6 MHz. A rotation diagram constructed from the data on

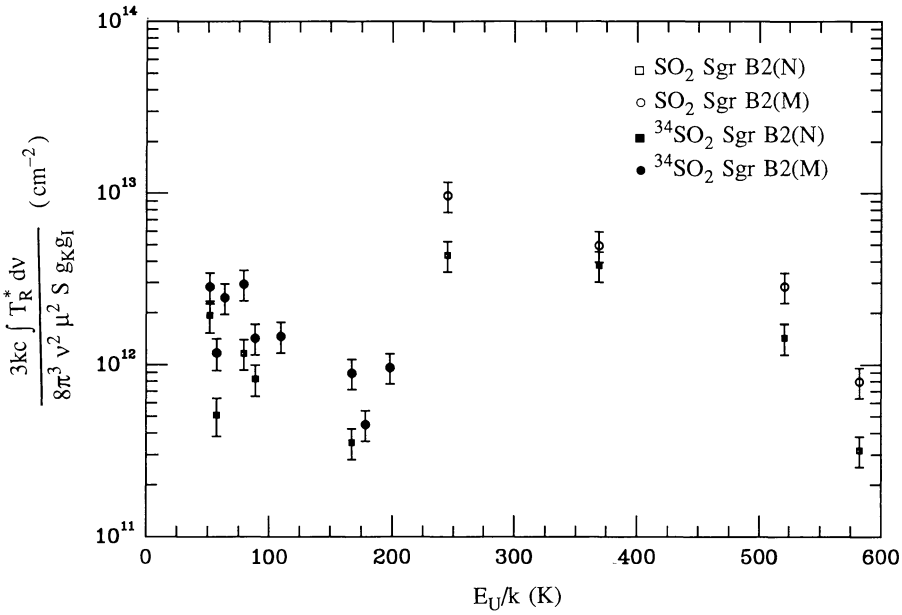

FIG. 11.—Rotation diagram for SO_2 and $^{34}SO_2$ in Sgr B2(M) and Sgr B2(N) based on JCMT data

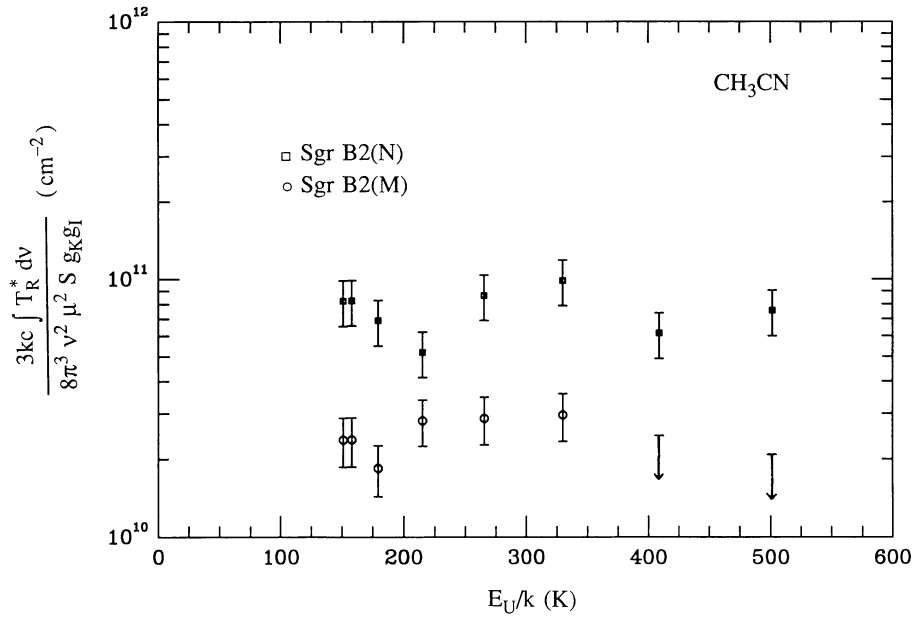

FIG. 12.—Rotation diagram for CH_3CN in Sgr B2(M) (*open circles*) and Sgr B2(N) (*open squares*), based on JCMT data

Sgr B2(N) gives a rotational temperature of 48.7 ± 6.4 K and a column density of $2.41 \pm 0.98 \times 10^{16}$ cm^{-2}, roughly 10 times the column density Turner deduced for Sgr B2(M) using a considerably larger beam. Our observations of Sgr B2(M) do not show any emission for the two higher energy transitions, but weak emission in the lowest energy transition. Adopting a rotational temperature of 49 K (in agreement with Turner), our single point implies a column density for Sgr B2(M) of 1.8×10^{15} cm^{-2}, exactly the result obtained by Turner, suggesting that the CH_3OCH_3 emission might be spatially extended, in contrast to its behavior in other sources such as Orion. It is clear that Sgr B2(N) has a higher column density of CH_3OCH_3 than Sgr B2(M), as well as higher excitation.

Formamide (NH_2CHO) was not detected in the CSO survey data for Sgr B2(M). In the JCMT survey data it is also not seen convincingly in Sgr B2(M), although it is seen clearly in Sgr B2(N). This is due to a combination of circumstances. The JCMT observations include data from the 318 GHz region where the $J = 15$–14 *a*-type band of NH_2CHO is located. The $J = 15$ levels of formamide lie in the 200–400 K range and are reasonably well populated in the high-excitation core of Sgr B2(N). Other lower-lying *b*-type transitions are also seen just in Sgr B2(N), indicating that NH_2CHO probably has a higher column density in the northern source as well. A single-component rotation diagram fitted to the data for Sgr B2(N) yields a rotational temperature of 89.3 ± 5.6 K and a column density of $2.56 \pm 0.45 \times 10^{15}$ cm^{-2}. The weak *b*-type transitions appear anomalously strong in our rotation diagram. This is similar to the effect seen by Turner (1991), who for this species favors non-LTE "pumping" instead of large opacities to explain this anomalous behavior. Our column density is much higher than Turner's 2.1×10^{14} cm^{-2}, suggesting that there is significant clumping of the NH_2CHO.

We seem to detect C_3H_2 in these observations in the direction of both Sgr B2(M) and Sgr B2(N), although it is weak in both sources. The intensities observed are consistent with the CSO observations discussed in § 3. Assuming similar excitation (~27 K), we derive column densities of order 1×10^{14} cm^{-2} toward Sgr B2(M) and 2×10^{14} cm^{-2} toward Sgr B2(N). The emission seen may be associated not with the cores at all but with foreground material.

Peculiar behavior is seen for the single line of HNCO in this data set ($15_{1,14}$–$14_{1,13}$). As shown in Figure 10*c*, this line is blended with the $K = 6$ $J = 18$–17 transition of CH_3CN. Decomposition of this blend into its two components is based on three considerations: (1) its intensity relative to the $K = 5$ line of CH_3CN, (2) the center frequency of the blended profile, and (3) the width of the blended profile. In Sgr B2(M) the observed line is centered on the HNCO frequency, and it is several times brighter than $K = 5$ CH_3CN. Only a small fraction of the blend can be attributed to CH_3CN. The profile is broad, possibly indicating the presence of a third, unidentified line. Otherwise the bulk of the intensity must be attributed to HNCO. The situation is reversed in the northern source. There the blended line is centered on the CH_3CN frequency, and its intensity is consistent with the other K components of CH_3CN (the degeneracy of the $K = 6$ line is twice that of $K = 5$ or $K = 7$). The profile is quite narrow, and HNCO would create a distinct high-frequency wing. Little HNCO emission seems to be present unless the velocity structure of HNCO in Sgr B2(N) is considerably different from that of CH_3CN. This behavior of HNCO [strong in Sgr B2(M) and weak in Sgr B2(N)] is opposite to that seen by Goldsmith et al. (1987), which is particularly surprising, since ours is a higher energy line than that observed by Goldsmith et al. Other aspects of this anomalous behavior of HNCO were discussed above in § 3.9.

5. DISCUSSION

5.1. *Chemistry*

The overall chemical properties of Sgr B2, as determined from the CSO survey data, are summarized in Table 7. In this

TABLE 7

MOLECULAR PARAMETERS FOR SAGITTARIUS B2(M)[a]

Molecule	T_{rot}[b] (K)	N_{MB} (cm^{-2})	$f = N/N(H_2)$[c]	v_{lsr} (km s^{-1})	ΔV (km s^{-1})	Notes
CO	(20)	1.3×10^{20}	5.2×10^{-5}	59.9	16.4	
CS	(20)	1.1×10^{16}	4.3×10^{-9}	60.7	22.8	d
SiO	(50)	4.0×10^{13}	1.5×10^{-11}	57.7	20.1	
SO	89	2.5×10^{16}	9.5×10^{-9}	59.4	19.2	e
NO	(20)	4.0×10^{16}	1.5×10^{-8}	61.0	≈ 19	
CN	(10)	$\approx 2.3 \times 10^{15}$	$\approx 8.8 \times 10^{-10}$	...	...	
C_2H	(20)	1.5×10^{15}	5.7×10^{-10}	58.5	15.6	
OCS	(200)	2.5×10^{15}	9.5×10^{-10}	62.0	15.8	
HCN	(20)	8.4×10^{15}	3.2×10^{-9}	62.8	36.6	
HNC	(20)	2.5×10^{15}	9.5×10^{-10}	59.4	20.1	
HCO^+	(20)	1.3×10^{15}	4.8×10^{-10}	60.1	13.6	
HCS^+	(20)	8.9×10^{13}	3.4×10^{-11}	64.0	12.1	f
HC_3N	14 (70)	4.3×10^{14} 4.9×10^{14}	3.6×10^{-10}	62.5	12.8	g
CH_3CN	...	...	...	62.2	17.5	h
CH_3OH	(10) 17 93	7.6×10^{15} 4.7×10^{16} 6.8×10^{15}	2.4×10^{-8}	63.1	15.9	
SO_2	153	4.7×10^{16}	1.8×10^{-8}	59.4	19.0	e
HNCO	20 (70)	1.8×10^{15} 1.3×10^{15}	1.2×10^{-9}	58.7	18.5	g
H_2CO	(20)	3.6×10^{15}	1.4×10^{-9}	60.8	17.4	
H_2CS	87	7.9×10^{14}	3.0×10^{-10}	58.9	19.6	
C_3H_2	27	1.6×10^{14}	6.3×10^{-11}	58.0	...	
CH_2CO	(71)	7.4×10^{14}	2.9×10^{-10}	...	19.8	
CH_2NH	(20)	8.6×10^{14}	3.3×10^{-10}	65	...	i

[a] Derived from CSO survey data.
[b] Temperatures in parentheses are assumed values.
[c] Assuming $N(H_2) = 2.6 \times 10^{24}$ cm^{-2}.
[d] $N_{MB} = 4.0 \times 10^{15}$ cm^{-2} if $T_{rot} = 50$ K.
[e] Includes correction for saturation.
[f] $N_{MB} = 2.5 \times 10^{13}$ cm^{-2} if $T_{rot} = 50$ K.
[g] Data on cool component from Turner 1991.
[h] Abundance uncertain because of complex excitation.
[i] Excludes cold component seen in absorption.

table we have taken the column densities derived in § 3 (based on the T_R^* scale), and converted them to average main-beam column densities by multiplying them by $(\eta_C)^{-1} = 1.9$. Thus the values shown are presented on the same basis as in Table 7 of Turner (1991). We have also converted these to fractional abundances $f(X) = N(X)/N(H_2)$ assuming an H_2 column density of 2.6×10^{24} cm^{-2} for Sgr B2(M) (Lis & Goldsmith 1990). It cannot be overemphasized that a great deal of caution must be used in interpreting these and other determinations of chemical abundances. These numbers often refer to particular components of the gas (particular temperature regions) which are different for different molecules. In some cases these figures significantly underestimate the column density because of inadequate sampling of the various excitation conditions by the available submillimeter lines. In Table 7 we have attempted to note some of the factors leading to uncertainties in our derived abundances. Absent from this table are most of the more complex molecular forms known to be present in Sgr B2. As discussed previously, submillimeter observations are strongly biased against detection of most such species.

Broadly speaking, the abundances shown for Sgr B2(M) are in the general range seen in previous observations of this source and also within the range of values predicted by models of interstellar cloud chemistry (Herbst & Leung 1986; Langer & Graedel 1989; Gredel et al. 1989). The abundances of several simple molecules are also quite similar to those observed in other sources such as TMC-1 and the extended ridge source in Orion. For example, the observed abundances of CO, CS, and HCN are all within a factor of a few of each other in these sources and in good agreement with the model predictions. As was the case for Orion and TMC-1, the greatest differences between the various sources and the models arise in carbon-rich species such as C_3H_2 and in more complicated molecules such as methanol.

Indeed, the observed abundances (or upper limits) for species such as HC_3N and C_3H_2 are quite similar for Sgr B2(M) and the extended ridge source in OMC-1, while the abundances in TMC-1 are some one to two orders of magnitude larger. The Sgr B2(M) values are far easier to account for in steady state models of interstellar chemistry. Models at early evolution times are required to explain the high hydrocarbon abundances in TMC-1.

The greatest differences for Sgr B2(M) and OMC-1 arise in molecules thought to have their abundances peaked in interaction regions between the outflowing wind from young, massive stars and their natal molecular cloud. Species such as SiO, SO_2,

and CH_3OH, which are found in rather compact sources in OMC-1, all have abundances there which are larger than those derived here for Sgr B2(M), by factors ranging from several to over 1000. In this regard it is important to note that our abundances in Sgr B2(M) are typically larger than those deduced from lower frequency observations with their characteristically larger beam sizes. Indeed, the sizes of the "perturbed" regions in Orion would only be some 1″–5″ at the distance of Sgr B2 and would still suffer considerable beam dilution, even in the present surveys.

Turner (1991) has advanced the thesis that the chemistries of Sgr B2 and OMC-1 are not as different as previously thought. Indeed, he proposes that the primary observational differences between these sources are due to the larger size of Sgr B2 and its greater distance. In this picture, previous observations of Sgr B2 have been dominated by emission from rather cool material in the extended cloud. Hot core sources have had comparatively less influence on the observations because of the large distance to the source and consequent beam dilution of these cores. Thus species such as HNCO, which are more abundant in Sgr B2 than in Orion, are found to be so because they are found predominantly in cooler cloud environments. Conversely, species such as SO_2 are more abundant in OMC-1 because they are associated with the compact region in the Orion core. If this view is correct, our current observations of Sgr B2 with a smaller beam size should reveal a more Orion-like chemistry. As discussed above, this does in fact seem to be the case. Observations at lower frequencies with beam sizes matched to the 345 GHz CSO survey (e.g., at 3 mm with the IRAM telescope or at 1.3 mm with the JCMT) would be most helpful in placing much tighter constraints on the abundances of heavier molecules to which we are not sensitive. Such abundances could then be directly compared with those reported here. Observations at still higher resolution would probably lead to an even greater similarity in the abundances of molecules such as SO_2 and CH_3OH in Orion and Sagittarius.

5.2. *Differences between Sgr B2(N) and Sgr B2(M)*

It is clear that there are considerable spectral differences between Sgr B2(M) and Sgr B2(N). These may be caused by differences in either excitation or molecular abundance, although these two factors are strongly interrelated in the interpretation of most of the observational data. Earlier evidence for higher excitation in the northern source came from the detection of vibrationally excited emission from HC_3N (Goldsmith et al. 1987). More recently it has become clear that both Sgr B2(M) and Sgr B2(N) are high-excitation regions, both for lines which are collisionally excited and for those which are radiatively excited (Lis & Goldsmith 1991). Indications are that although Sgr B2(N) has higher excitation than Sgr B2(M), *both* regions have peak densities of order 10^7 cm^{-3} and are subject to radiation fields with temperatures on the order of 260 K. The data reported here confirm this picture, with detection of many highly excited lines in both sources. Our data are consistent with somewhat higher excitation in Sgr B2(N).

There also appear to be differences in molecular column density between the two sources. It is evident just from Figure 10 that there are considerably more lines in Sgr B2(N) than in Sgr B2(M) and that these lines are typically stronger. Quantitatively, for most species the integrated intensities of lines in Sgr B2(N) are between 2 and 10 times higher than for those in Sgr B2(M). Any differences in excitation will affect the relationship between integrated intensity and column density. However, assuming similar excitation in the two sources, it would appear that for most species, column densities are of order 5 times larger in the northern source than in the middle source. Such a ratio is consistent with the difference in H_2 column density derived from thermal dust emission (Martín-Pintado et al. 1990). Despite this general correlation with H_2 column density, it is clear that the abundances of some species do not track that of H_2 in detail. Lis & Goldsmith (1991) find that HC_3N emission is not well correlated with that of $C^{18}O$ and conclude that the fractional abundance of HC_3N varies by a factor of about 3 on a 1′ scale.

The principal departure from the pattern of higher abundances in the north is for the species SO and SO_2, which seem to be from 2 to 10 times *less* abundant in Sgr B2(N) than in Sgr B2(M). In OMC-1 these molecules are found in the plateau source, where they are thought to be part of a high-velocity outflow originating from IRc2. The chemistry of this region is known to be considerably different from that of the rest of the Orion cloud, in part because of shock-induced chemistry, although some of the differences may be related to the high-temperature environment at the base of the outflow region. It is possible that Sgr B2(M) is in some ways similar to the Orion plateau, with a sulfur-dominated chemistry in a region where an outflow source is developing. This would be consistent with the view (e.g., Vogel et al. 1987) that Sgr B2(M) is in a more advanced evolutionary state than Sgr B2(N), a state in which the material around the core is beginning to be dispersed.

5.3. *Kinematics*

In Table 7 we have also listed the kinematic information derived from the CSO survey data. The average v_{lsr} for those molecules detected in Sgr B2(M) is 60.6 km s^{-1}, consistent with the results of Cummins et al. (1986) and Turner (1991). There are statistically significant variations in the v_{lsr} of certain molecules. For example, we and the two previous surveys agree that the species SO, SO_2, and H_2CS show emission somewhat blueshifted from the mean velocity of the cloud (except for SO_2, on which Turner disagrees). This may be related to the other chemical differences observed for these species, particularly the fact that SO and SO_2, which peak on the middle source (M), are clearly associated with a different component of the gas. We and Cummins et al. also see significantly blueshifted emission from SiO. Noticeably redshifted emission occurs for OCS, a conclusion with which all three surveys agree. For the remaining molecules there is less general agreement, probably because of the different energy levels sampled in the three surveys and velocity differences between the cooler and hotter components of the gas.

The average velocity width (FWHM) from our Sgr B2(M) data is 18.5 km s^{-1}, somewhat less than the averages from Cummins et al. and Turner. There is little consistency among the surveys other than a general trend toward greater widths for SO, H_2CS, and HNCO and narrower lines for CH_3OH. It also

appears that the ionized species (HCO^+ and possibly HCS^+) may have significantly narrower line widths, a reasonable result given that they likely exist in different regions than the neutral material.

It is known that there is a north-south velocity gradient in Sgr B2, giving rise to a different mean velocity for Sgr B2(N) than for Sgr B2(M). Our observations of Sgr B2(N) give a mean v_{lsr} of 65.2 km s^{-1}, similar to previous results. The mean line width in the observations of Sgr B2(N) is 13.8 km s^{-1} (FWHM), slightly narrower than that seen in the CSO data on Sgr B2(M), possibly because of the smaller JCMT beam size. However, inspection of Figure 10 reveals that there do seem to be a number of features in Sgr B2(N) that are narrower than anything seen in Sgr B2(M), even at similar spatial resolution. Among these are the CH_3OCH_3 lines. Dimethyl ether is an abundant species in the Orion compact ridge source, a quiescent, warm, oxygen-rich source with large abundances of complex molecules. This suggests that there may be a region akin to the Orion compact ridge in the vicinity of Sgr B2(N).

6. SUMMARY

In this work we have surveyed submillimeter molecular line emission in the direction of dense cores in Sgr B2. The chemical picture derived for this region is significantly different from that derived from previous lower spatial resolution observations. It is clear that molecular clouds in general, and Sgr B2 in particular, exhibit sharp variations in chemical composition on small spatial scales. Thus observations at high resolution are important, since much interesting detail about the chemistry is lost at low resolution. It seems clear that interferometry will become increasingly important in the study of cloud chemistry. However, it is important that the use of interferometric resolution be combined with the study of a sufficient number of transitions to obtain an accurate picture of the distribution of population among the various molecular levels.

Because of a general correlation, for most molecules, between line frequency and excitation energy, high-frequency observations are best suited for studying hot core sources and are poorly suited for observing cooler diffuse material. Further, it is clear that the high-frequency lines of many molecular species become optically thick in these dense cores. Interpretation of the opacity then becomes of considerable importance in deriving molecular abundances, the ultimate test of our understanding of star formation and the structure and chemistry of molecular clouds.

This work has been supported in part by the National Science Foundation under grants AST-8715295, AST-8818327, and AST-9196077. One of the authors (W. C. D.) has received funding through the L. W. Frohlich Research Fellowship of the New York Academy of Sciences, and another (P. A. J.) has been supported by NASA's Graduate Student Researchers Program. G. A. B. would like to thank the David and Lucille Packard and Alfred P. Sloan Foundations for their support. Research at the Caltech Submillimeter Observatory has been funded by NSF grants AST-8311849 and AST-8815132. The James Clerk Maxwell Telescope is operated by the Royal Observatory Edinburgh on behalf of the Science and Engineering Research Council of the United Kingdom, the Netherlands Organization for Scientific Research, and the National Research Council of Canada. We are most grateful to Colin Masson and Antony Schinkel for their help with the CSO observations and to Adrian Russell and Göran Sandell for their assistance at the JCMT. This manuscript has benefited from helpful comments by L. E. Snyder and the referee, B. E. Turner.

REFERENCES

Batrla, W., Matthews, H. E., Menten, K. M., & Walmsley, C. M. 1987, Nature, 326, 49
Botschwina, P. 1989, Ion and Cluster Ion Spectroscopy and Structure, ed. J. P. Maier (New York: Elsevier), 59
Carlstrom, J. E., & Vogel, S. N. 1989, ApJ, 337, 408
Carroll, T. J., & Goldsmith, P. F. 1981, ApJ, 245, 891
Churchwell, E., Wood, D., Myers, P. C., & Myers R. V. 1986, ApJ, 305, 405
Cummins, S. E., Green, S., Thaddeus, P., & Linke, R. A. 1983, ApJ, 266, 331
Cummins, S. E., Linke, R. A., & Thaddeus, P. 1986, ApJS, 60, 819
Elmegreen, B. G., Genzel, R., Moran, J. M., Reid, M. J., & Walker, R. C. 1980, ApJ, 241, 1007
Goldsmith, P. F., Langer, W. D., Elldér, J., Irvine, W. M., & Kollberg, E. 1981, ApJ, 249, 524
Goldsmith, P. F., Lis, D. C., Hills, R., & Lasenby, J. 1990, ApJ, 350, 186
Goldsmith, P. F., Snell, R. L., Hasegawa, T., & Ukita, N. 1987, ApJ, 314, 525
Gredel, R., Lepp, S., Dalgarno, A., & Herbst, E. 1989, ApJ, 347, 289
Herbst, E. 1990, private communication
Herbst, E., & Leung, C. M. 1986, ApJ, 310, 378
Irvine, W. M., & Schloerb, F. P. 1984, ApJ, 282, 516
Jewell, P. R., Hollis, J. M., Lovas, F. J., & Snyder, L. E. 1989, ApJS, 70, 833
Langer, W. D., & Graedel, T. E. 1989, ApJS, 69, 241
Lis, D. C., & Goldsmith, P. F. 1990, ApJ, 356, 195
———. 1991, ApJ, 369, 157
Lis, D. C., Goldsmith, P. F., Scoville, N. Z., & Carlstrom, J. E. 1991, in preparation
Loren, R. B., & Mundy, L. G. 1984, ApJ, 286, 232
Martín-Pintado, J., de Vicente, P., Wilson, T. L., & Johnston, K. J. 1990, A&A, 236, 193
Menten, K. M., Walmsley, C. M., Henkel, C., & Wilson, T. L. 1986a, A&A, 157, 318
Menten, K. M., Walmsley, C. M., Henkel, C., Wilson, T. L., Snyder, L. E., Hollis, J. M., & Lovas, F. J. 1986b, A&A, 169, 271
Millar, T. J., Bennett, A., & Herbst, E. 1989, ApJ, 340, 906
Snyder, L. E., Kuan, Y.-J., & Pratap, P. 1991, in Skylines: Proc. Third Haystack Observatory Meeting, ed. A. D. Haschick & P. T. P. Ho, in press
Sutton, E. C., Blake, G. A., Genzel, R., Masson, C. R., & Phillips, T. G. 1986, ApJ, 311, 921
Sutton, E. C., Blake, G. A., Masson, C. R., & Phillips, T. G. 1985, ApJS, 58, 341
Sutton, E. C., Danchi, W. C., Jaminet, P. A., & Ono, R. H. 1990b, Internat. J. Infrared Millimeter Waves, 11, 133
Sutton, E. C., Jaminet, P. A., Danchi, W. C., Masson, C. R., & Blake, G. A. 1990a, in Kona Symposium on Millimetre and Submillimetre Astronomy, ed. G. D. Watt & A. S. Webster (Dordrecht: Kluwer), 105
Turner, B. E. 1989, ApJS, 70, 539
———. 1990, ApJ, 362, L29
———. 1991, ApJS, 76, 617
Vogel, S. N., Genzel, R., & Palmer, P. 1987, ApJ, 316, 243
Wannier, P. G. 1980, ARA&A, 18, 399
———. 1989, in IAU Symposium 136, The Center of the Galaxy, ed. M. Morris (Dordrecht: Kluwer), 107
Wright, M. C. H., & Vogel, S. N. 1985, ApJ, 297, L11
Ziurys, L. M., Friberg, P., & Irvine, W. M. 1989, ApJ, 343, 201